UNIVERSIDADE DE LISBOA
FACULDADE DE CIÊNCIAS
DEPARTAMENTO DE QUÍMICA E BIOQUÍMICA

Activation and Conversion of Small Molecules by Coordination Compounds

Janaína de Cássia Almeida

Mestrado em Química
Especialização em Química

Dissertação orientada por:
Paulo Nuno Martinho
Sara Realista

2018

To my mother, Lenita Dias,

who always makes me believe in my dreams ♥

Acknowledgements

I would like to thank my supervisor, Dr. Paulo Nuno Martinho, first for the chance to work with him, for all advices, guidance and opportunities. Mainly, for the contribution in my scientific development, ideas and suggestions. Also, for the patience and understanding. It was such a pleasure working with that great human being and I am extremely grateful for the experience of constant learning.

I sincerely thank my co-supervisor, Dr. Sara Realista for the encouragement, for having a lot of patience (yes, I know). Thank for the lessons, the instructions, the contribution in my scientific development. Thanks for the time spent teaching me, the joy, the reprimands, thanks for make me grow. I do not have enough words to express my gratitude! Thanks for everything! You have a special place in my heart.

“The good teacher explains. The superior teacher demonstrates. The great teach inspires.” (William Arthur Ward) And with no doubts, both supervisors have inspired me. You are the best!

I would also like to express my gratitude to Prof. Dr. Maria José Calhorda, for the opportunity of work in inorganic and theoretical group and for attention being given.

I am thankful to Dr. Marta Saraiva for the assistance provided in the laboratory, to Dr. Ana Mourato for the AAS experiments and to Prof. Dr. Ana Maria Rego for the XPS analysis and the consideration given.

Many thanks to all my laboratory colleagues: Ana Elisa, Ana Vicente, Bárbara Oliveira, Mohamed Soliman, Frederico Martins, César Reis, Rafaela Marques, Marcos Bento e Olga Ferreira. You all contribute for the amazing life in this laboratory. Thanks for all contributions and the good energies.

Quero agradecer de coração à minha querida mãe, Lenita Dias, a quem dedico esta tese. Agradeço por me ter transmitido valores essenciais, por desde sempre ter me ensinado grandes lições e acima de tudo por sempre acreditar em mim e no meu potencial. Estou imensamente grata por me ter ensinado a batalhar e a nunca desistir dos meus sonhos! Também agradeço ao meu querido pai, Geraldo Almeida, pelo carinho transmitido.

Many thanks to my friends: Jéssica Sodré, Sofia Milheiro, Tânia Simões, Bianca Gama, Mirian Vaz e Tânia Ferreira for the support, the understanding and your presence in good and bad moments.

A special thanks to my boyfriend Pedro Rocha for all the patience, for giving me strength in the stressfully days and for all the support. Thank you for always believe in me and for make me a better person. You are amazing!

Abstract

Chapter 1 of this master thesis consists of a brief introduction concerning the activation and conversion of small molecules, specially the carbon dioxide molecule. The class of macrocyclic compounds studied in this thesis is also described, as well as the literature evolution along the years and the most common procedures for their synthesis. A special emphasis can be found on some of the different existing azamacrocycles. Another topic addressed is the ability of macrocycles to encapsulate the carbon dioxide molecule and to reduce this gas photochemically in homogeneous phase. Finally, an example of covalent immobilisation of a cryptate on multi-walled carbon nanotubes is discussed.

During this work ten compounds were synthesised, six new compounds (two ligands and four complexes) and four other compounds already published by our group. The characterisation was performed by nuclear magnetic resonance (NMR), *Fourier*-transform infrared spectroscopy (FTIR) and elemental analysis (EA) and these techniques showed that the compounds were successfully obtained. The synthesis and characterisation are presented in **Chapter 2**. Two complexes synthesised during my bachelor's degree research project are presented in this chapter, as they were further used as catalysts for carbon dioxide photoreduction studies. In general, the yields were satisfactory obtained above 45%.

The covalent immobilisation of **C3** on carbon nanotubes was studied and the synthesis and characterisation are described in **Chapter 3**. Characterisation techniques such as atomic absorption spectroscopy (AAS) and X-ray photoelectron spectroscopy (XPS) were employed to fully characterise all synthetic steps. These revealed that the immobilisation occurred, however large amounts of copper were found in the material due to their use as a catalyst in the last step of the cryptate immobilisation.

CO_2 photoreduction studies were performed using nickel(II) and cobalt(II) complexes as catalysts in homogeneous medium and the results are discussed in **Chapter 4**. Two different set-ups were used for this purpose. One was composed by three blue LED lights source (λ= 492-455 nm) and the other was composed by a solar light simulator (λ= 400-750 nm). Tests were accomplished with different pairs of photosensitiser/sacrificial donor. To analyse the headspace gases produced, a GC-TCD was used and the liquid phase was first analysed by ionic chromatography, although without success. As an alternative, a qualitative evaluation of the presence of liquid CO_2 reduction products was carried out by a ^{1}H NMR method based on the literature. This showed that among the analysed samples only in two was detected formic acid.

A heterogeneous photoreduction experiment was also performed using as catalyst the modified carbon nanotube with **C3**. The gaseous phase was analysed by GC-TCD and only showed H_2 as by-product and no CO_2 photoreduction products were observed. Thus, further studies are still needed with different amounts of catalyst, different systems of PS/SD and solvents.

Finally, in **Chapter 5** are presented the main conclusions and future work and in **Chapter 6** is found the detailed description of the synthesis and characterisation of all compounds studied.

Keywords: CO_2, macrocycles, homogeneous catalysis, metal complexes and photoreduction.

Resumo

O crescimento populacional a nível mundial tem resultado num aumento das diversas formas de poluição. Neste sentido, a comunidade científica tem revelado um interesse crescente em combater a poluição atmosférica devido ao aumento de gases poluentes tais como CO_2, NO_x, SO_2, CH_4, entre outros. Diversos estudos têm sido realizados numa tentativa de minimizar as emissões e a acumulação de dióxido de carbono na atmosfera, existindo principalmente três estratégias: redução da quantidade de dióxido de carbono produzida, a utilização do dióxido de carbono sob a forma de matéria-prima e o armazenamento desse gás. Diversos investigadores têm procurado novos catalisadores que possuam eficiência e durabilidade e que tenham a capacidade de ativar e/ou converter seletivamente a molécula de CO_2.

No âmbito desta tese de mestrado é apresentada, no **Capítulo 1**, uma breve introdução sobre a ativação e conversão de pequenas moléculas, mais especificamente para a molécula do dióxido de carbono. Neste capítulo, também se encontra a descrição de compostos macrocíclicos (classe de compostos onde se inserem os compostos estudados), o surgimento destes no decorrer da história e as formas mais comuns para a sua síntese. Tendo em conta os compostos estudados nesta tese, é realizada uma discussão mais profunda de alguns azamacrociclos existentes. Outro tema abordado relaciona-se com a encapsulação da molécula de dióxido de carbono em compostos macrociclícos e é descrita a sua redução fotoquímica, em fase homogénea. Por fim, é dada uma pequena discussão sobre a imobilização covalente de compostos em nanotubos de carbono para a sua utilização em catálise heterogénea.

No decorrer do trabalho foram sintetizados dez compostos, seis compostos novos (dois ligandos e quatro complexos) e quatro compostos já publicados pelo nosso grupo. Os ligandos novos sintetizados pertencem à classe de compostos tipo pinça, sendo um de cadeia aberta (**L1**) e outro um macrociclo (**L2**). O macrociclo foi complexado com Ni(II) e Co(II) dando origem a dois complexos novos (**C1** e **C2**, respetivamente). Também foram sintetizados dois criptatos novos de Ni(II) (**C3**) e Co(II) (**C4**), com um grupo funcional C≡H nos anéis aromáticos do criptato. Os quatro compostos sintetizados, anteriormente reportados pelo nosso grupo, são dois criptandos com Br como substituinte nos anéis aromáticos, (**L3** e **L4**) e os seus respetivos criptatos de Ni(II) (**C5**) e Co(II) (**C6**). A síntese e caracterização dos compostos é descrita no **Capítulo 2**. A caracterização foi efetuada por ressonância magnética nuclear (NMR), espetroscopia de infravermelho com transformada de *Fourier* (FTIR) e análise elementar (EA) e estas técnicas permitiram concluir que as sínteses dos compostos foram bem-sucedidas, tendo-se obtido os compostos pretendidos. De uma forma geral, os rendimentos obtidos foram satisfatórios sendo o seu valor acima dos 45%. Dois complexos sintetizados durante o meu projeto final de licenciatura (**C7** e **C8**) foram utilizados como catalisadores para os estudos de fotorredução do dióxido de carbono.

Com o intuito de fazer um material com um destes compostos para a sua aplicação em catálise heterogénea, foi estudada a imobilização covalente do criptato de níquel(II) (**C3**) em nanotubos de carbono. A síntese e caracterização deste novo material é descrita no **Capítulo 3** onde são discutidas também técnicas de caracterização como espectroscopia de absorção atómica (AAS) e espectroscopia de fotoeletrões de raios-X (XPS). Estas experiências revelaram que a imobilização ocorreu, todavia, grandes quantidades de cobre(II) foram encontradas no material sintetizado devido à sua utilização como catalisador no último passo da reação.

Estudos de fotorredução foram realizados utilizando complexos de níquel(II) e cobalto(II) como catalisadores em meio homogéneo e os resultados são apresentados no **Capítulo 4**. Para tal foram utilizadas duas montagens diferentes construídas no nosso laboratório para a realização destes ensaios.

A montagem I tinha na sua constituição um compartimento com um conjunto de três lâmpadas LED azuis (λ=492-455 nm) onde os ensaios foram realizados por seis horas. **A montagem II** é constituída por uma lâmpada capaz de simular o espectro solar (λ=400-750 nm) com uma duração de irradiação de setenta e duas horas. Foram realizados ensaios com diferentes pares de fotossensibilizador/dador sacrificial verificando-se que com os pares purpurina/trietilamina (TEA), 9-antracenocarbonitrilo/TEA, purpurina/BIH, $[Ru(phen)_3]_2(PF_6)_2$/BIH/TEOA não foram observados produtos gasosos da fotorredução do dióxido de carbono. Apenas para o par $[Ru(phen)_3](PF_6)_2$/TEOA se obtiveram resultados e os produtos gasosos foram analisados por GC-TCD. Relativamente aos produtos líquidos utilizou-se a cromatografia iónica para a deteção dos mesmos, porém a utilização desta última técnica não foi bem-sucedida. Como alternativa, realizou-se uma análise qualitativa dos produtos líquidos por ressonância magnética nuclear de protão (^{1}H NMR) tendo como base uma experiência realizada na literatura. Esta permitiu concluir que das amostras analisadas, apenas duas apresentavam ácido fórmico como produto da fotorredução de CO_2.

Os ensaios deveriam ter sido realizados no mínimo três vezes para cada amostra, mas por falta de tempo tal não foi possível. Em regra, os complexos de cobalto(II) apresentaram melhores resultados que os complexos de níquel(II) nos dois sistemas. Para a **montagem I**, o melhor TON_{CO} foi obtido utilizando o criptato de cobalto(II) com brometo como substituinte nos anéis aromáticos (**C6**) como catalisador. De forma geral, para este sistema os valores de seletividade foram bons sendo entre 84-97%. Para a **montagem II**, na maior parte dos casos, também se verificou que os complexos de cobalto(II) tinham melhores resultados comparativamente aos complexos de niquel(II). Mais uma vez, o complexo (**C6**) demonstrou ser o melhor catalisador dos compostos em estudo, porém com um valor de seletividade para o CO extremamente baixo. Os restantes valores de seletividade para o CO estavam compreendidos entre 43-97%. Neste sistema observou-se a presença de metano no complexo **C6**, com um valor de TON_{CH_4} e seletividade muito baixos. Mais estudos são necessários para averiguar se os restantes catalisadores também são capazes de produzir este gás. Os criptatos de cobalto(II) com grupos desactivadores como substituinte (Br) (**C5** e **C6**) mostraram ter valores maiores de TON_{CO} e TOF_{CO} em relação aos com grupos ativadores (C≡CH) e ao com grupo neutro (H). Por outro lado, os criptatos de níquel(II) com grupos ativadores (C≡CH) (**C3** e **C4**) tiveram melhores resultados do que os criptatos com os outros substituintes. Para os macrociclos do tipo pinça os resultados foram semelhantes com melhores resultados de TON_{CO}, TOF_{CO} e Φ_{CO} para o complexo de cobalto(II) do que para o complexo de níquel(II).

Um trabalho mais aprofundado será necessário para verificar a eficiência e durabilidade dos diferentes catalisadores, como por exemplo, estudos com diferentes concentrações de catalisador e ensaios com um maior tempo de irradiação.

Realizou-se também, um ensaio de fotorredução em fase heterogénea utilizando como catalisador os nanotubos de carbonos imobilizados com o criptato **C3**, utilizando a **montagem I**. A fase gasosa analisada por GC-TCD apenas revelou a presença de H_2 como subproduto e nenhum produto da fotoredução do CO_2 foi observado. Mais estudos serão necessários com diferentes concentrações de catalisador, diferentes pares de fotosensibilizador/redutor sacrificial e solventes para se confirmar que este material não dá origem a produtos provenientes da fotorredução do dióxido de carbono.

Por fim, no **Capítulo 5** são apresentadas as conclusões e perspetivas do trabalho realizado nesta tese de mestrado e no **Capítulo 6** são apresentadas as sínteses completas dos diversos compostos assim como a sua caracterização.

Palavras-chave: CO_2, criptandos, catálise homogénea, complexos metálicos e fotorredução.

Table of Contents

List of illustrations

Tables index

Index of schemes

Symbols and abbreviations

$\bar{\nu}$	wavenumbers
^{13}C-APT NMR	carbon nuclear magnetic resonance (Attached Proton Test)
^{1}H-NMR	proton nuclear magnetic resonance
9CNA	9-antharacenecarbonitrile
AAS	atomic absorption
Asc	ascorbic acid
BIH	1,3-dimethyl-2-phenyl-2,3-dihydro-1H-benzo[d]imidazole
bipy	2,2' – bipyridine
BNH	1-benzyl-1,4-dihydronicotinamide
Boc	*tert*-butyloxycarbonyl
C.A.C.T.I.	Centro de Apoyo Científico y Tecnológico a la Investigación
CAT	catalyst
cm^{-1}	wavenumber units
COSY	Correlation Spectroscopy
DCM	dichloromethane
DFT	density functional theory
DMF	dimethylformamide
DPA	2,6-Pyridinecarboxylic acid
EA	Elemental Analysis
eq	equivalent
ESI-MS	Electrospray Ionisation Mass Spectroscopy
FTIR	*Fourier*-Transform Infrared Spectroscopy
GC-TCD	Gas Chromatography Thermal Conductivity Detector
h^{-1}	per hour
HMBC	Heteronuclear Multiple Bond Connectivity
HMQC	Heteronuclear Multiple Quantum Coherence
h	hour
LED	light-emitting diode
MWCN	multi-walled carbon nanotubes
NMP	N-2-methyl pyrrolidone
NMR	nuclear magnetic resonance
phen	1,10-phenantroline
ppm	units of NMR chemical shift
ppy	phenylpyridine
PS	photosensitiser
r.t	room temperature
SD	sacrificial donor
TEA	triethylamine
TEOA	triethanolamine
TMEDA	tetramethylethylenediamine
TOF	turnover number
TON	turnover frequency
TPP	tetraphenylporphyrin

TREN	tris(2-aminoethyl)-amine
TREN	tris(2-aminoethyl)amine
V	volt
W	watt
XPS	X-ray photoelectron spectroscopy
δ	chemical shift
δ_{x-x}	bending vibration of function group X-X
λ	wavelength
υ	stretching vibration
Φ	quantum yield

Chapter 1
Introduction

1. Introduction

1.1 Activation and conversion of small molecules

The scientific community has been constantly searching for new efficient and durable catalysts with the ability of activate, convert small molecules such as H_2, H_2O, O_2, N_2, CO_2, etc. These molecules have a significant impact in areas such as biology, medicine, environmental protection and industrial catalysis.[1] Two conversion processes are frequently used: electro- and photocatalysis. They are used for a sustainable and reversible conversion of energy into chemicals and can operate under homogeneous or heterogeneous media.[2]

There is a huge concentration of efforts to find new catalysts bearing non-noble metal ions due to their abundance and low-cost. A problem that arises from the use of non-noble metals catalysts is their common low reactivity when compared to the noble-metals catalysts. Metal ions and compounds including macrocyclic complexes have a crucial role in photochemical activation and conversion of small molecules when acting as catalysts.[2]

This thesis will focus on the activation and conversion of carbon dioxide, which is considered a greenhouse gas and its concentration has been continuously increasing in the atmosphere with dramatic consequences for earth's delicate synergies. In this line of action, both new earth abundant metal catalysts and other known catalysts were studied for their ability to photoreduce CO_2.

1.2 Macrocycles

A macrocycle compound can be described as a cyclic compound with nine or more atoms (including all heteroatoms) and with at least three donor atoms.[3] The macrocycles are important and powerful ligands due to two main reasons: i) they have the capacity to thermodynamically and kinetically stabilise metal complexes and ii) they can mimic important biological systems found in nature, like the porphyrin unit of many metalloproteins.[4]

In 1967 Pedersen[5] reported for the first time the synthesis of thirty three cyclic polyethers macrocyclic ligands. In **Figure 1.1** is some examples of the cyclic polyethers synthesised, some of them formed stable complexes with several cations such as Li^+, Na^+, K^+, Ag(I), Au(I), Hg(I), Hg(II), Tl(I), Ce(III), Pb(II) and others.

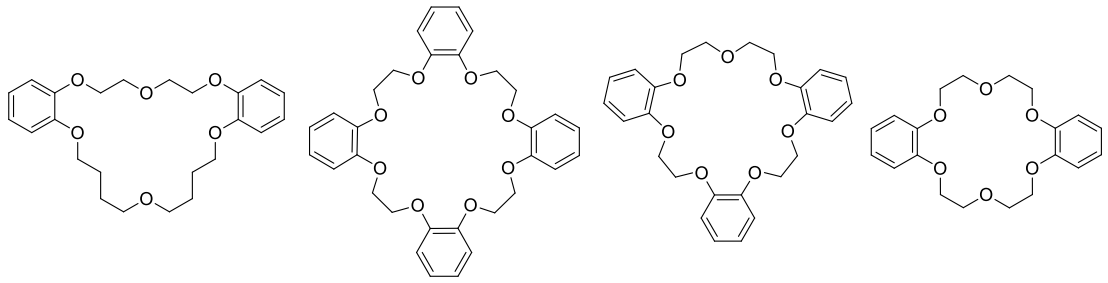

Figure 1.1 – Examples of macrocycles synthesised by Pedersen.[5]

Important conclusions concerning the conditions for the formation and the factors influencing the stability of these polyether complexes were discovered. These include the relative size of the ion and the size of the cavity in the polyether ring, the tendency of the ion to interact with the solvent molecules, the electrical charge on the ion, the number of oxygen atoms in the polyether ring, among others. In that time, another significant result was the understanding that a stable complex is not formed if the ion is too large to fit in the cavity of the polyether ring.[5]

Afterwards, many other macrocyclic ligands have been synthesised and their properties investigated.[6–9] An interesting aspect of these ligands is their ability to coordinate different metal ions, therefore giving rise to different applications which resulted in increasing their attention along the years. Most importantly, the size of the metal ion and the macrocycle cavity that are crucial for the designing of macrocyclic metal complexes.[5]

The macrocyclic ligands can be synthesised by two different methods: 1) The metal-ion-template or 2) in high dilution organic chemistry pathway. In **Scheme 1.1** is depicted the synthesis of a crown ether using the template method. The synthesis can lead to a polymeric side-product instead of forming the desired crown ether. This difference is related to the ability of K^+ to organise the reactants to give a proper intermediate that is pre-organised to form the crown ether. The NEt_3 base is not as efficient to form this intermediate as KOH and the reaction takes an intermolecular instead of intramolecular pathway. If we wish to induce the formation of a host that is selective for a specific compound, we have to use an ion with similar size as that of the final compound.[10] When a suitable template is not formed, the synthesis of macrocyclic ligands are much more difficult and high-dilution conditions must be employed. In diluted solutions the formation of the cyclic product by intramolecular reactions is more likely to occur (**Scheme 1.2**).[10]

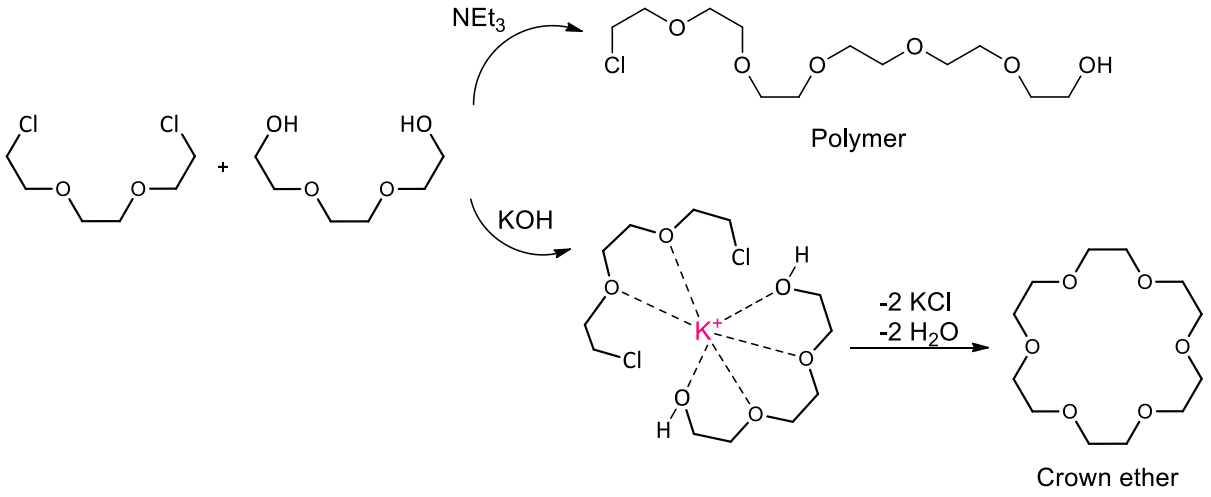

Scheme 1.1– Possible pathway leading to cyclic and acyclic products in the synthesis of [18]crown-6. Adapted from ref.[10]

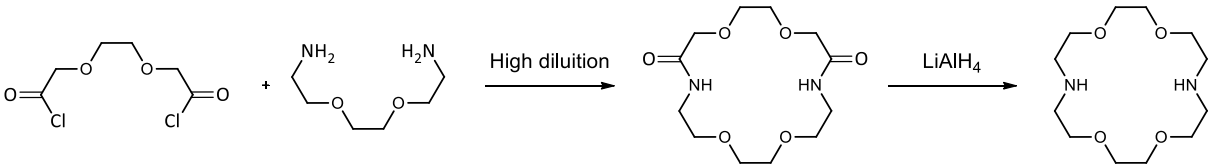

Scheme 1.2 – High-dilution synthesis of diaza[18]crown-6. Adapted from ref.[10]

Macrocyclic ligands comprising heteroatoms are important due to increasing their diversity towards different species (cations, anions and neutral molecules). Azamacrocycles contain nitrogen atoms in their structure. Usually these types of ligands are more available for compounds that do not form stable complexes with macrocycles containing oxygen atoms.

The first macrocycle containing amine groups was the tetraazaquaterene, synthesised by Baeyer in 1886 (**Figure 1.2(a)**). Years later, Alphen reported a new type of cyclic amines: the cyclams (**Figure 1.2(b)**).[11]

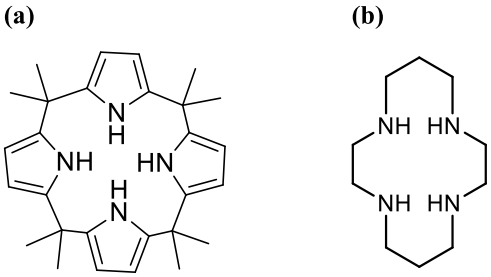

Figure 1.2– Tetraazaquaterene (a) and (b) cyclam.

Throughout the years different azamacrocycles were synthesised. In **Figure 1.3** are depicted some examples of azamacrocycles synthesised by several authors.

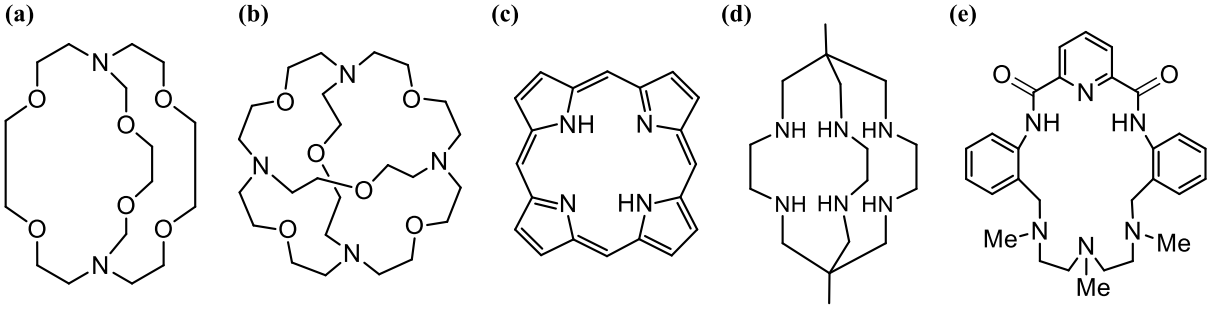

Figure 1.3– Examples of azamacrocyclic compounds: a), b) cryptands, c) porphyrin, d) tetraazamacrocycle and e) macrocycle ligand with an NNN-pincer moiety [4,10,12,13]

Jean-Marie Lehn, Nobel prize winner in chemistry, introduced in 1969 a new class of macrocycles, the cryptands[14] (**Figure 1.3(a)**, **(b)**). According to IUPAC nomenclature, cryptands are molecular entities containing cyclic or polycyclic assemblies of three or more binding sites held together by covalent bonds. These structures comprise a molecular cavity that allows the encapsulation of other molecules (guest), including cations, anions or neutral species. When a cryptand coordinates one or several metal cations a cryptate is formed.

After these first reports, a huge diversity of cryptands with different modifications such as multiple bridges have been synthesised, e.g. “soccer ball cryptand” (**Figure 1.3(b)**).[10] Cryptates have also been synthesised and two examples can be visualised in **Figure 1.4**.

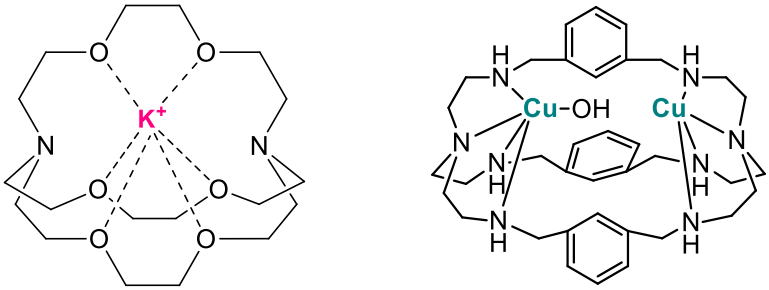

Figure 1.4– Examples of cryptates.[15,16]

Another type of very well-known azamacrocycles are porphyrins **Figure 1.3(c).** This type of ligands have been extensively studied due to their ability to coordinate metal ions yielding complexes with interesting and relevant properties (e.g. heme, chlorophyll and phthalocyanine blue).[13] (**Figure 1.5**).

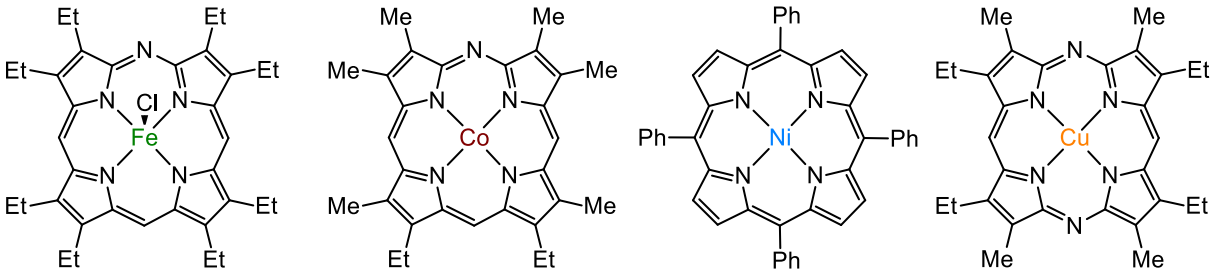

Figure 1.5– Examples of porphyrin complexes. Adapted from ref.[13]

An example of a macrobicyclic ligand may be viewed as a tetraazamacrocycle spanned by a bis-donor bridge connected to carbon bridgehead atoms as shown in **Figure 1.3(d)**. The metal coordination is represented in **Figure 1.6**.

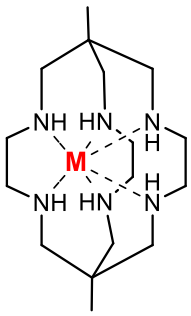

Figure 1.6 – Clathochelate metal coordination.

Finally, in **Figure 1.3(e)** a macrocycle ligand with an NNN-pincer moiety is represented. Pincer ligands gained attention in 1976 when Shaw and co-workers first synthesised this type of compounds.[17] The structure of pincer type complexes is based on a metallic centre and a pincer type ligand that comprises donor atoms (D in **Figure 1.7**) in its structure that are able to coordinate to a metal ion in a tridentate fashion. The name changes according to donor atoms present, for example compounds having phosphorus in their structure are called PCP pincer complexes.[18] Therefore several pincer ligands such as CCC[19,20], NCN[21,22], PCN[23,24], OCO[25], SPS[26], etc. have been synthesised and studied in different catalytic applications.

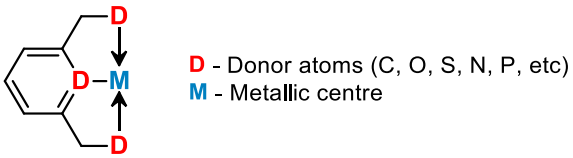

Figure 1.7 – Structure of a pincer ligand**.** Adapt from ref.[18]

The Ni-Fe-S enzyme, carbon monoxide dehydrogenase has in its catalytic site (C-cluster) Ni(II)···(HO)-Fe(II) bridge moiety that catalyses the $CO + H_2O \rightleftharpoons CO_2 + 2H^+ + 2e^-$ reaction. Holm and co-workers[12] saw this as an opportunity to produce a new set of macrocycles and complexes with a proximal Ni···Cu bridge formation and a pincer binding site. Moreover, changing the aromatic or aliphatic substituents can lead to variable and/or improved properties of the complexes. Two examples of the complexes synthesised can be observed in **Figure 1.8**.

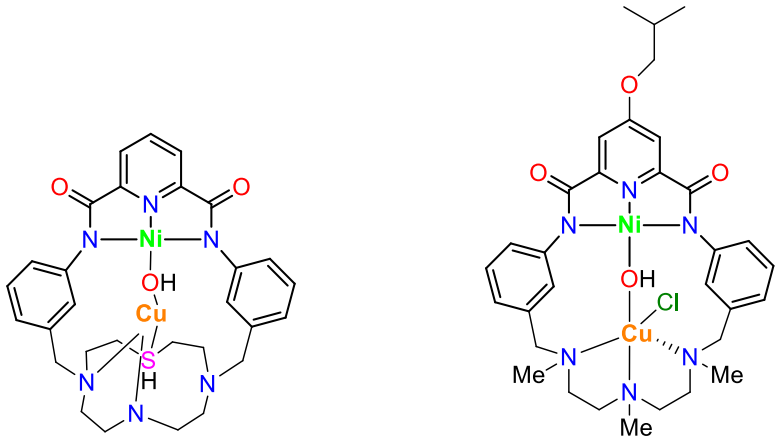

Figure 1.8– NNN-pincer complexes synthesised by Holm and co-workers.[12]

1.3 Encapsulation of CO_2

As previously stated, Holm and co-workers synthesised and studied NNN-pincer acyclic and macrocyclic Ni(II) complexes.[27,28] In 2011, they synthesised eleven NNN-pincer Ni(II) complexes with different substituents such as, Me, Et, Pr^i, among others (**Figure 1.9**). Additionally, two macrocyclic Ni(II) complexes with NNN-pincer moieties were synthesised (**Figure 1.10**). They found that these complexes react easily and completely with carbon dioxide in DMF solution in a process of CO_2 fixation yielding bicarbonate complexes. The structure of seven complexes, four with -OH and three with $-CO_3H$ were obtained by X-ray diffraction. The reaction mechanism was also proposed based on DFT methods for the R=Pr^i system. Kinetic studies were performed in the same year[29] and thermodynamic studies were deeply investigated.[30] These studies were performed to understand the reaction mechanism.

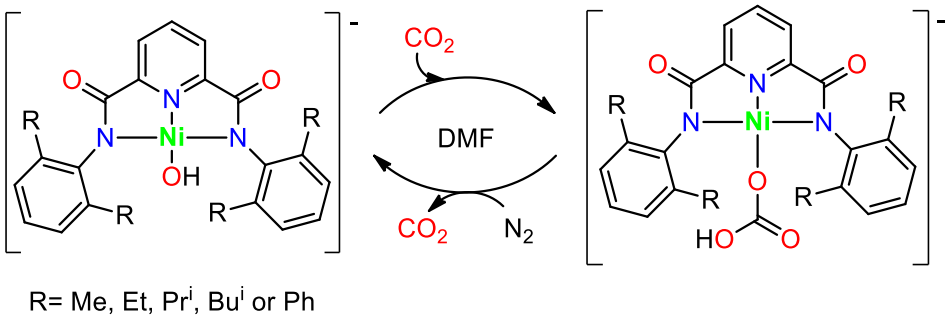

Figure 1.9 – CO_2 fixation reactions of the NNN-pincer acyclic complexes synthesised by Holm and co-workers. Adapted from ref.[29]

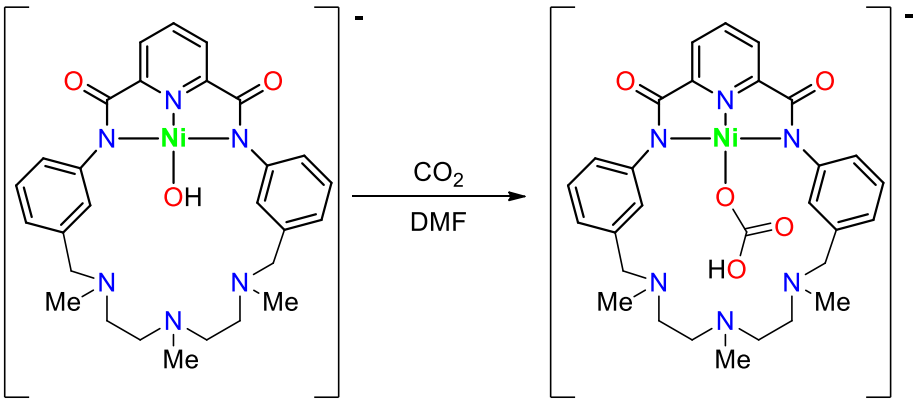

Figure 1.10– CO_2 fixation reactions of the NNN-pincer macrocyclic complex synthesised by Holm and co-workers. Adapted from ref.[28]

In 2014, Bowman-James and co-workers[31] reported a bis(carboxamide) ligand that is able to capture atmospheric CO_2 (confirmed by ESI-MS) and stabilise it in the macrocyclic cavity as a carbamate (N-CO_2) (**Figure 1.11**).

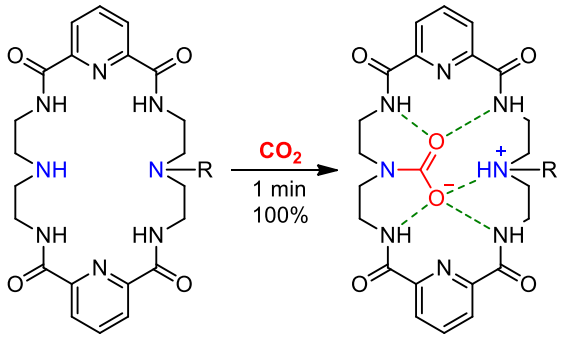

Figure 1.11– Structure of NNN-pincer macrocycles synthesised by Kristin research group. Adapted from ref.[31]

Murray and co-workers[32] synthesised one ligand with three NNN-pincer moieties. This ligand was used to synthesise two complexes, one of Ni(II) and a second of Cu(II) (**Figure 1.12**). The Ni(II) complex shows two metallic centres instead of the expected three metallic centres coordinated to the three pincer moieties. This complex shows a bicarbonate molecule coordinated to one Ni(II) centre and a hydroxide bound to the other Ni(II) centre. This is the only example where both terminal Ni−OH and Ni−OCO_2H coexist in the same complex. The authors investigated the CO_2 release and realise that the bicarbonate cannot be released as CO_2 either thermally or upon sparging with N_2. Similarly to the Ni(II) complex, the Cu(II) compound (**Figure 1.12**) shows two metallic centres coordinated to only two NNN-pincer moieties. This third metal centre helps to stabilise a carbonate molecule and two hydroxides that are coordinated to the metal centres. They concluded that the carbonate or bicarbonate was captured from atmospheric CO_2.

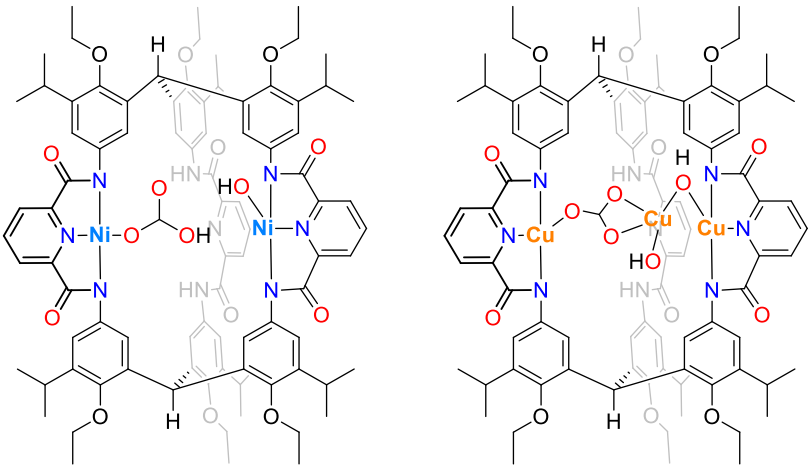

Figure 1.12 – Ni(II) (left) and Cu(II) (right) complexes synthesised by Murray research group.[32]

Nelson and co-workers[33] synthesised octazacryptates capable of coordinate two metal centres such as Ni(II), Cu(II), Co(II) and Zn(II), which are based in cascade complexation. This type of complexation was introduced in the literature by Lehn and was denoted as Lehn's strategy (**Figure 1.13**) and consists on the anions bridging which allows the coordination of two metal centres.[34]

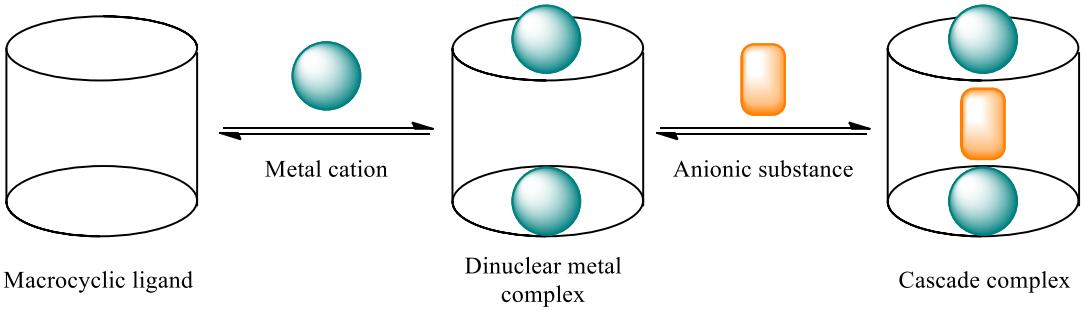

Figure 1.13 – Representation of Lehn's strategy. Adapted from ref.[34]

Additionally, Nelson and co-workers, found that these structures can convert atmospheric CO_2 into carbonates. The encapsulation of CO_2 can occur in different bridging modes. In **Figure 1.14** are the bridging modes discovered through X-ray crystallography.

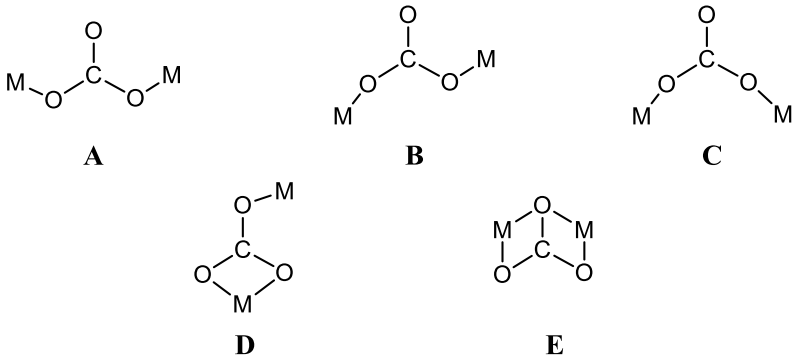

Figure 1.14 – Carbonate bridging modes in Jane Nelson's octazacryptates.[33]

The bridging mode depends on the metal ion used and for Cu(II) and Ni(II) complexes a coordination mode *anti-anti* η_1,η_1 is observed **Figure 1.14(A)**. For the Zn(II) cryptate a *syn-anti* μ-η_1,η_1 bridge mode **B** and for the Co(II) complexes **D** and **E** bridging modes were observed. The **C** mode was only observed for other anions than carbonate or bicarbonate are found between the metal centres.

Nelson's group also concluded that when methanolic solutions were used, methylcarbonate instead of carbonate was obtained. Later, Lu and co-workers[35] studied in more detail the Cu(II) cryptate with several primary alcohols in the reaction media including methanol, ethanol, propanol, butanol and 1,2-ethanediol. This study produced a mechanism of carbonate monoesters formation (**Figure 1.15**). First, the coordinated H_2O molecule loses a proton and the $[Cu_2(OH)L]^{3+}$ species are obtained. Then, the CO_2 carbon atom suffers a nucleophilic attack by OH^- and forms the $[Cu_2L(\mu\text{-}O_2COH^-)]^{3+}$ bridged cryptate. Finally, the primary alcohol attacks the carbon of the bicarbonate and the carbonate monoester is formed by water molecule elimination.

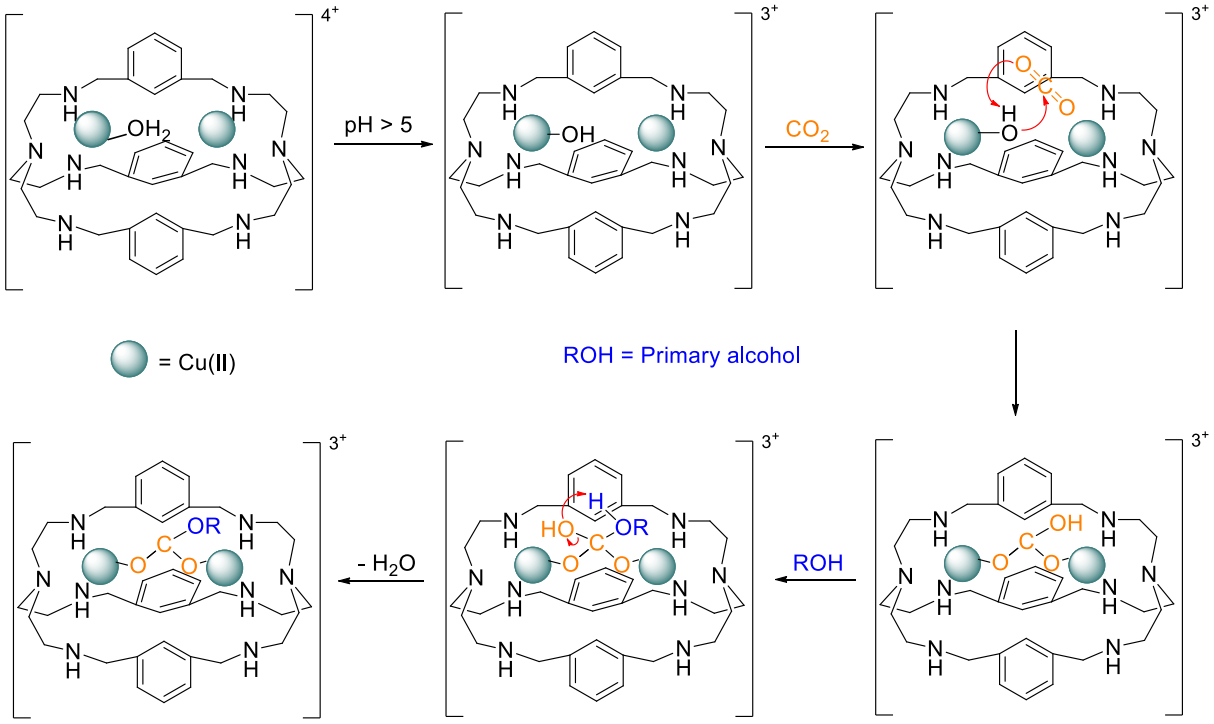

Figure 1.15 – Fixation and esterification of CO_2, mechanism proposed for Cu(II) cryptate. Adapted from ref.[35]

1.4 Photochemical reduction of CO_2

Recently, the increase of carbon dioxide concentration in the atmosphere has reached a point that results in severe climatic changes due to the greenhouse effect. The scientific community saw in this problem an opportunity to deeply study the chemistry of CO_2 conversion. Thus, artificial photosynthesis methods have been investigated to try to solve the pollution problems and the energy crisis. Artificial photosynthesis is a process capable of reproduce the photosynthesis phenomenon that consist in the production of energy from sunlight.

The reduction of CO_2 can produce multiple added value products such as CO, formic acid, methane, methanol and oxalate, being an attractive way to regenerate renewable fuels and reduce the amount of carbon dioxide in the atmosphere.[36–38] The equations with the products resulting from CO_2 reduction are in **Table 1.1.**

Table 1.1– Equations of CO_2 reduction products.

Reactions	$E^{0'}$ (V) vs SCE[a]
$CO_2 + 2H^+ + 2e^- \rightarrow HCO_2H$	-0.85
$CO_2 + 2H^+ + 2e^- \rightarrow CO + H_2O$	-0.77
$CO_2 + 8H^+ + 8e^- \rightarrow CH_4 + 2H_2O$	-0.48
$CO_2 + 4H^+ + 4e^- \rightarrow HCOH + H_2O$	-0.72
$CO_2 + 6H^+ + 6e^- \rightarrow CH_3OH + H_2O$	-0.62

[a] $E^{0'}$ potentials are reported at pH 7.

Artificial photosynthesis can be performed in heterogeneous or homogeneous media and the work described in this thesis is only devoted to the latter. The photocatalysis reactions can be divided in two types: 1) In type I two different molecules, a photosensitiser (PS, **Figure 1.16**), and a transition metal catalyst (CAT) work together, 2) In type II one molecule acts at same time as both PS and CAT.[39] Both

type I and type II use a molecular sacrificial donor (SD, **Figure 1.17**). Considering the scope of this thesis, only type I will be discussed.[37,40]

Type I photocatalysis starts with the promotion of the PS to an excited state PS* due to irradiation (**Scheme 1.3(a)(b)** step **1**). This excited state suffers a quenching that can be a reductive or oxidative quenching (**Scheme 1.3(a)(b)**). In **Scheme 1.3(a)** the excited state PS* is reductively quenched by the SD giving a reduced sensitiser PS^- (one electron-reduced species) and an oxidized amine donor $SD^{\bullet+}$ (**Scheme 1.3(a)** step **2**). Finally, as PS^- is a stronger reductant than PS and PS*, the electron can be donated to the CAT and the original PS state is regenerated and the catalytic cycle restarts (**Scheme 1.3(a)** step **3**). On the other hand in the oxidative quenching (**Scheme 1.3(b)**), the PS* will react first with the CAT that directly accepts an electron from PS* (**Scheme 1.3(b)** step **2**) originating PS^+ and $CAT^{\bullet-}$. This PS^+ species will return to its original state due to one-electron transfer from SD (**Scheme 1.3(b)** step **3**).[39,40]

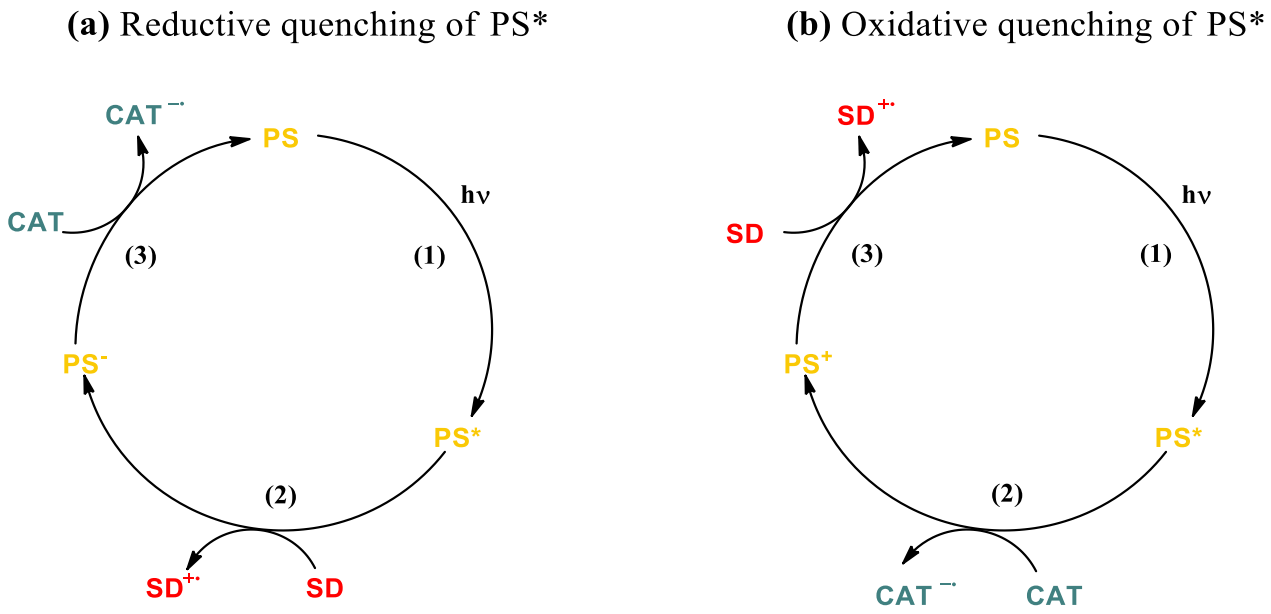

Scheme 1.3 – (a) Reductive and **(b)** oxidative quenching. Scheme adapted from literature. Adapted from ref.[40]

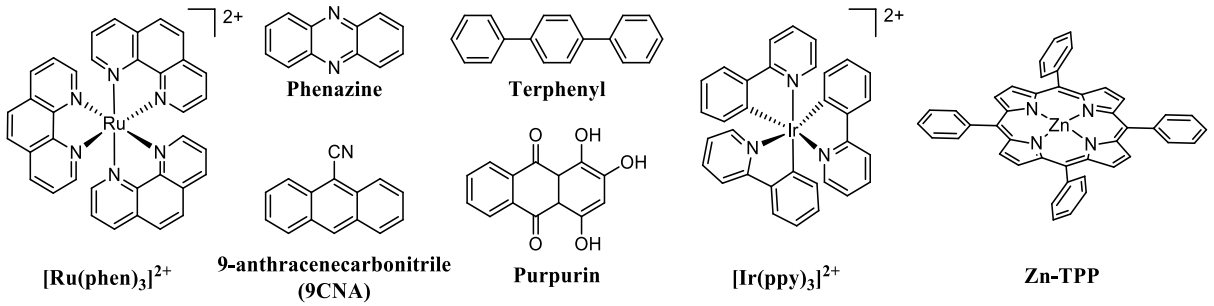

Figure 1.16– Examples of photosensitisers (PSs) used for CO_2 photoreduction.

Frequently, different sets of PS/SD (**Figure 1.16** and **Figure 1.17**) are used to ensure that the electron transfer occurs. $[Ru(phen)3]^{2+}$ is frequently used with triethanolamine (TEOA) as SD. Derivatives, such as $[Ru(bipy)_3)]^{2+}$ are used with ascorbic acid (Asc), TEOA and 1,3-dimethyl-2-phenyl-2,3-dihydro-1H-benzo[d]iidazole (BIH) as SD. The photosensitisers $[Ir(ppy)_3]^{2+}$, phenazine, 9-anthracenecarbonitrile (9CNA) and Zn-TPP are commonly used with triethylamine (TEA) as SD. The PS terphenyl can perform with TEA, TEOA and 1-benzyl-1,4-dihydronicotinamide (BNAH).

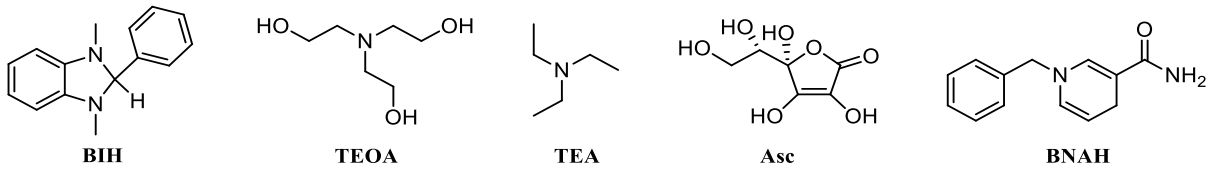

Figure 1.17– Sacrificial donors most used for CO_2 photoreduction.

As metal complexes have been used as highly selective catalysts for CO_2 photoreduction, strategies to immobilise them on materials have been applied. Modification of carbon nanotubes has been developed by scientists to attach non- and covalently metal complexes. This immobilisation allows the possibility of carrying out heterogeneous photocatalytic reactions, the advantage compared to homogeneous catalysis being a simple procedure for product/catalyst separation. Robert and co-workers[41] reported a MWCNT modification through the diazonium salt of paraphenylmethyl amine protected by *tert*-butyloxycarbonyl (Boc) (**Scheme 1.4**). The diazonium salt was chemically reduced releasing N_2 as a covalent bond between the aryl group and the MWCNT is formed. After, the amine function was deprotected to yield primary amine groups onto the surface that allows covalent attachment of the Fe(III) porphyrin catalyst (**Scheme 1.4**). The authors performed covalent grafting of the Fe(III) porphyrin catalyst onto MWCNT leading to an efficient electroreduction of CO_2 into CO in water with high selectivity.[41]

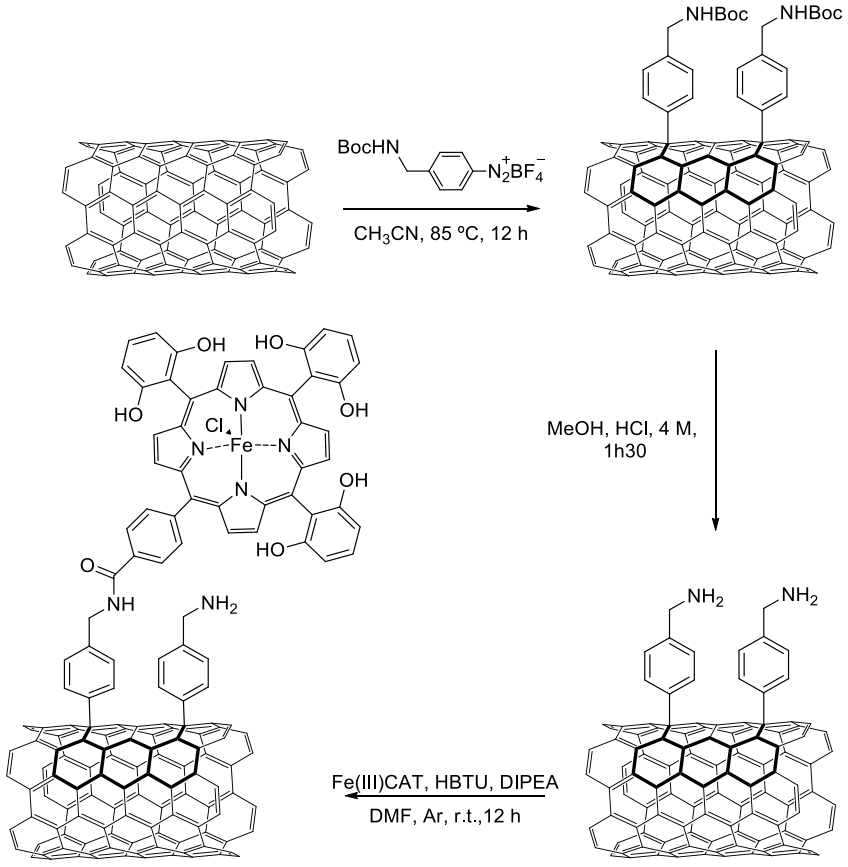

Scheme 1.4 – Covalent immobilisation of an Fe(III) porphyrin catalyst onto MWCNT. Adapted from ref.[41]

Chapter 2
Synthesis and characterisation

2. Synthesis and Characterisation

During this thesis ten compounds were synthesised included in two different classes of compounds that are pincer-based compounds and octaazacryptands.

Two new ligands pincer-like compounds were synthesised where one is an open chain ligand (**L1** in **Scheme 2.2**) and the other a macrocycle (**L2** in **Scheme 2.3**). The pincer-like macrocycle was coordinated to Ni(II) and Co(II) ions originating two new complexes (**C1** and **C2**, respectively **Scheme 2.5** and **Scheme 2.6**).

Two new octaazacryptates were also synthesised with Ni(II) (**C3** in **Scheme 2.7**) and Co(II) (**C4** in **Scheme 2.8**) ions, bearing a C≡H substituent on the aromatic ring of the octaazacryptands. However, the C≡H cryptand (**L6**) was previously synthesised by Sara Realista during her PhD thesis.[42] Finally, octaazacryptands previously reported by our group having a bromine substituent in the aromatic rings (**L3** and **L4**) and their Ni(II) and Co(II) cryptates (**C5** and **C6**) are synthesised and characterised.

The characterisation of the compounds was performed by nuclear magnetic resonance (NMR) spectroscopy, *Fourier*-transform infrared spectroscopy (FTIR) and elemental analysis (EA) and will be further discussed in detail.

2.1 Ligands synthesis

2.1.1 Pincer-like compounds

The precursor used for the synthesis of **L1** was dimethyl 2,6-pyridine dicarboxylate **E**, an ester obtained by esterification of 2,6-pyridinedicarboxylic acid (DPA) (**Scheme 2.1**), using a procedure from literature.[43]

Rybak-Akimova et al.[44] synthesised a macrocycle as result of a [2+2] cyclisation between 2,6-pyridine dicarboxylic acid ester and 1,4,7,10-tetraazadecane. To assure that the by-product [1+1] macrocycle was not obtained, the authors first isolated the [2+1] product (similar to **Scheme 2.2**) and only afterwards reacted it with 1 equivalent of the desired amine. An analogous procedure was performed to obtain ligand **L2**. (similar to **Scheme 2.3**).

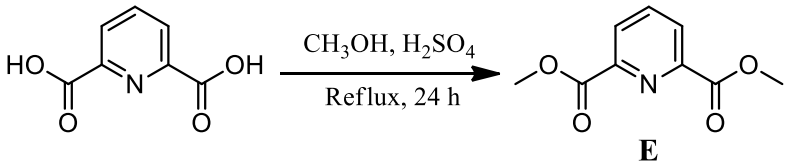

E

Scheme 2.1 – Synthetic pathway to obtain precursor **E**.

One equivalent of the ester compound was added to 0.27 equivalents of the amine to obtain the [2+1] compound, **L1**, the pincer-like open chain ligand (**Scheme 2.2**). The compound was isolated and purified before using it in the following reaction.

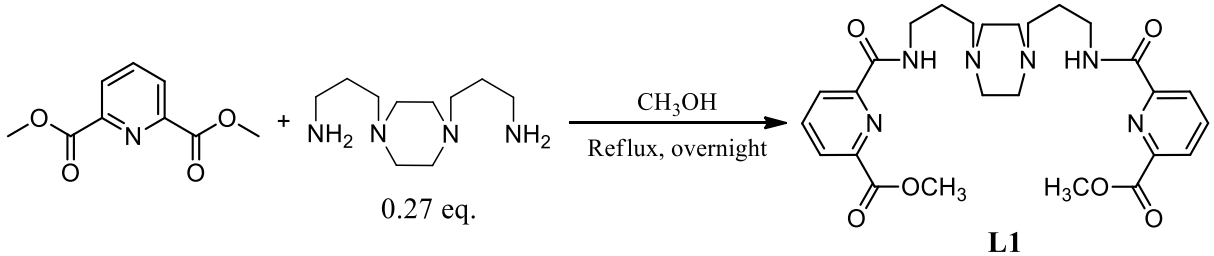

L1

Scheme 2.2 – Synthesis of the product of [2+1] condensation, **L1**.

The condensation to obtain **L2** was accomplished by the addition of 1 equivalent of the appropriate amine, 1,4-bis(3-aminopropyl)piperazine, to **L1** (**Scheme 2.3**).

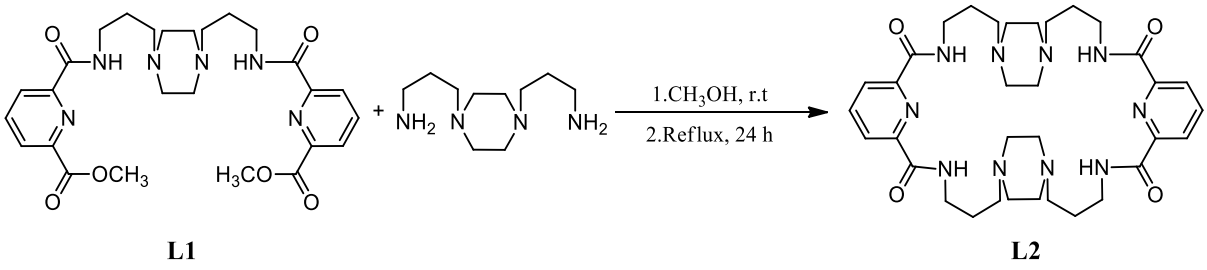

Scheme 2.3 – Synthesis of the macrocycle **L2.**

2.1.2 Cryptands

The reaction between an aldehyde (or a ketone) and an amine gives an hemiaminal. Hemiaminals of primary amine lose water to form a carbon-nitrogen double bond, an imine function (*Schiff* Base).[45] Reaction of three equivalents of an aldehyde with two equivalents of tris(2-aminoethyl)-amine (TREN) originates a cryptand (**L3** in **Scheme 2.4**).[16] The synthesis of **L4** (**Scheme 2.4**), a cryptand with amine functions, was possible by the reduction *Schiff* Base, with a specific reducing agent, $NaBH_3CN$.

Jane Nelson *et. al.*[33] synthesised similar compounds but without any type of substituent (**L5** in **Figure 2.1(a)**). To understand the influence of the substituents in the aromatic ring two different groups were introduced. The first one included an electron withdrawing group, bromide as substituent in the aromatic ring (**L3** and **L4 Scheme 2.4**), the second one is composed by an electron-donating substituent (C≡CH) (**L6** in **Figure 2.1(b)**).

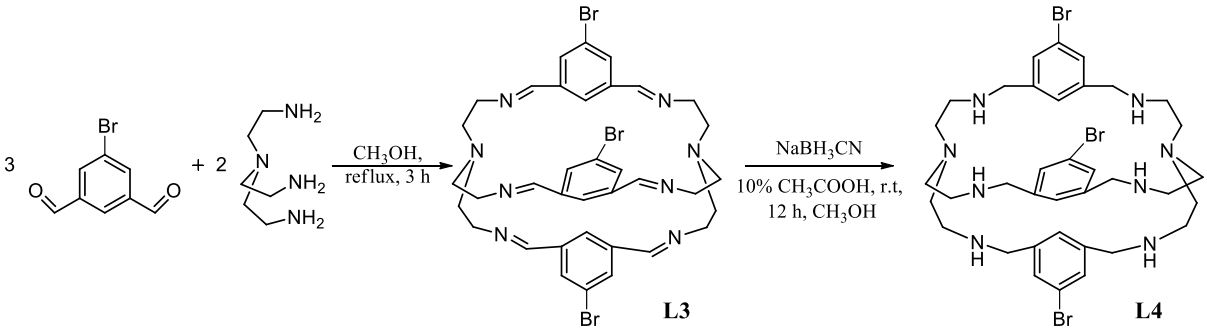

Scheme 2.4 – Synthetic pathway to obtain cryptands **L3** and **L4**.

In **Figure 2.1** the structure of the know cryptands **L5** and **L6** used to synthesise the cryptates (**C3**, **C4**, **C7** and **C8 Section 2.2.2 Cryptates**) and for CO_2 photoreduction studies is shown (**Chapter 4**).

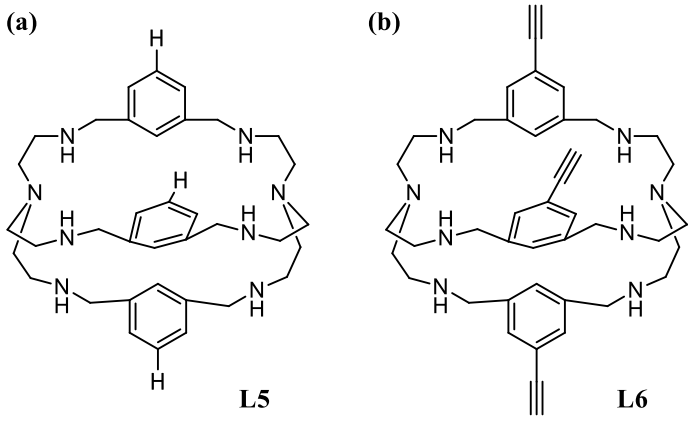

Figure 2.1 – Structure of Nelson's cryptand **L5 (a)** and cryptand **L6 (b)**.

2.2 Complexes synthesis

2.2.1 Pincer-like complexes

Coordination with transition metals using **L2** was performed by the addition of a metal salt. Two complexes were obtained from Ni(II) and Co(II), **C1** and **C2**, respectively, shown in **Scheme 2.5** and **Scheme 2.6**.

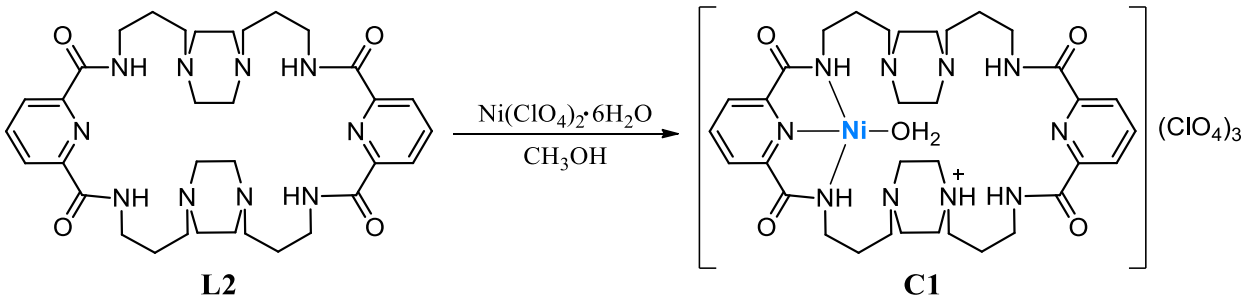

Scheme 2.5 – Synthesis of complex **C1**.

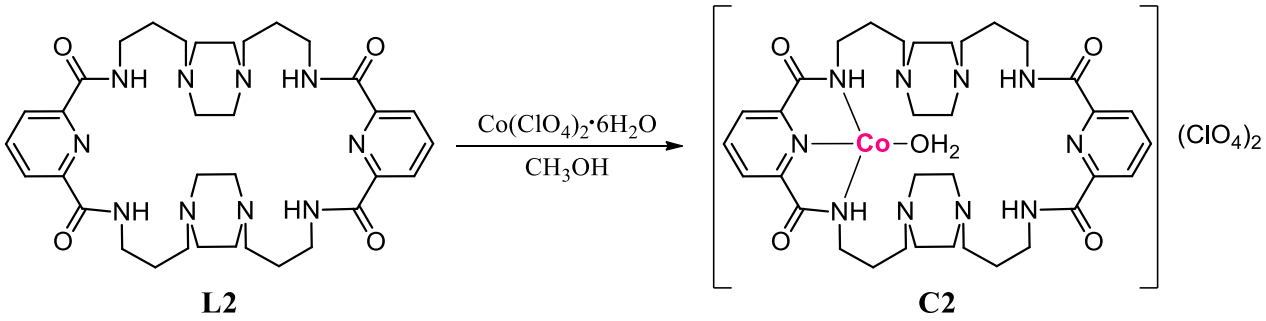

Scheme 2.6 – Synthetic pathway of **C2** complexation.

2.2.2 Cryptates

A cryptate can be formed by the addition of a metal salt to a cryptand. The metals are coordinated inside the cage (**Scheme 2.7**). The synthesis of the complexes **C3-C6** are represented in **Scheme 2.7-Scheme 2.10**.

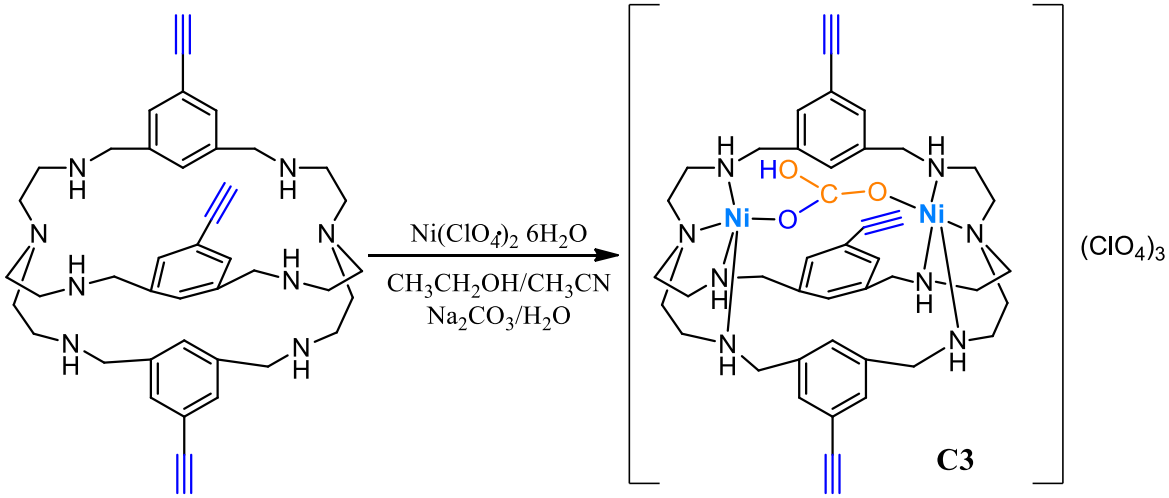

Scheme 2.7 – Synthesis of the cryptate **C3**.

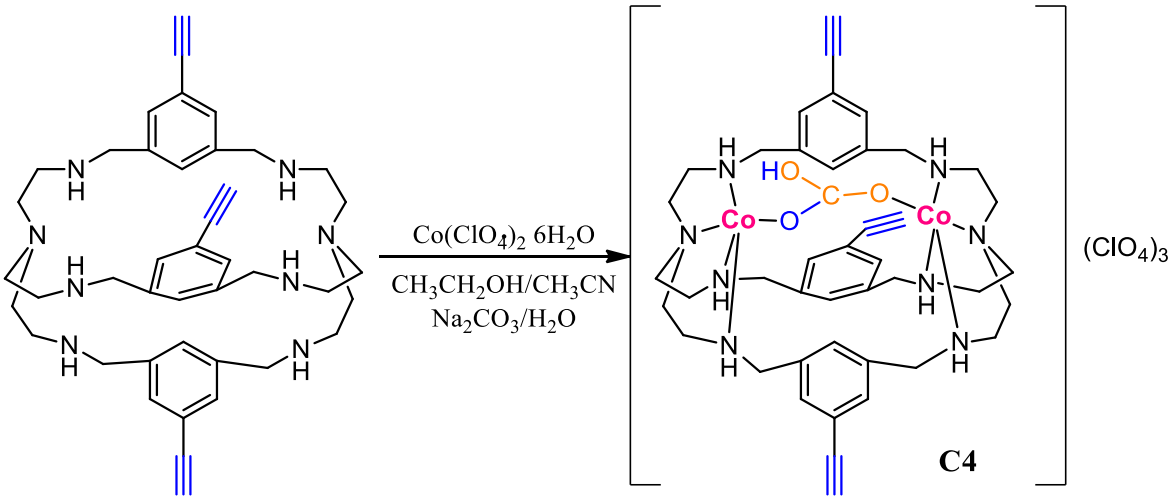

Scheme 2.8 – Synthesis of the cryptate **C4**.

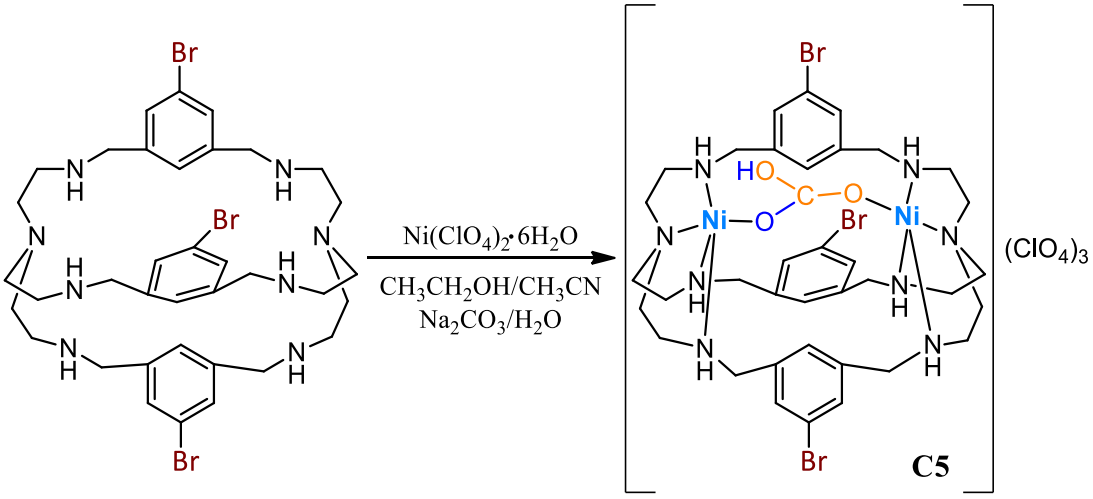

Scheme 2.9 – Synthesis of the cryptate **C5**.

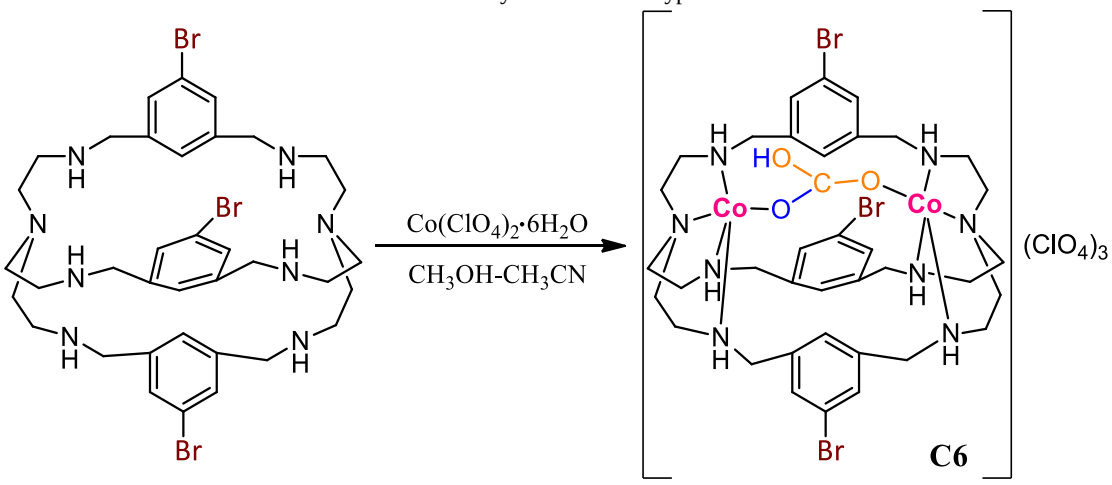

Scheme 2.10 – Synthesis of the cryptate **C6**.

The synthesis of two complexes, **C7** and **C8**, is showed in **Scheme 2.11-2.12**. These compounds were synthesised previously and will be used in this project as catalysts for the CO_2 photoreduction studies.

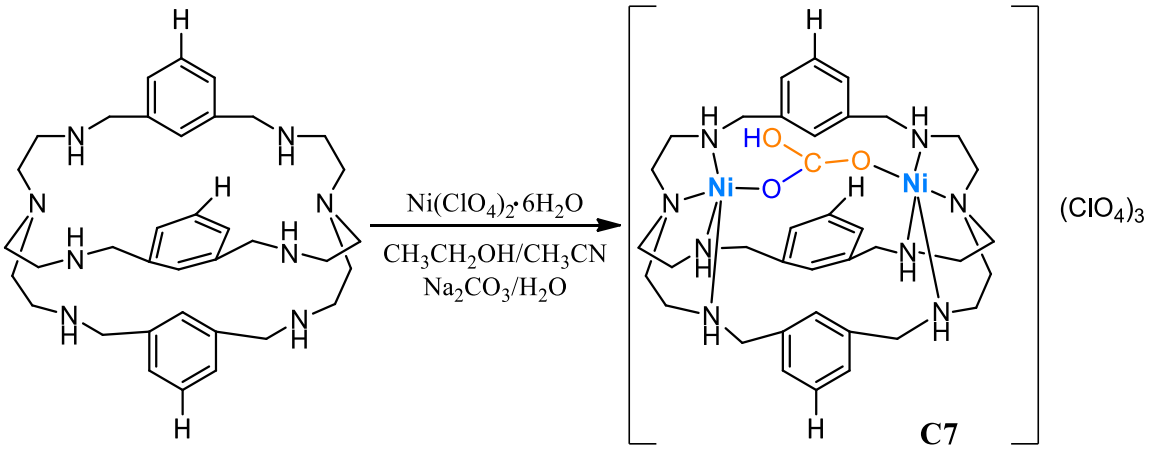

Scheme 2.11 – Synthesis of the cryptate **C7**.

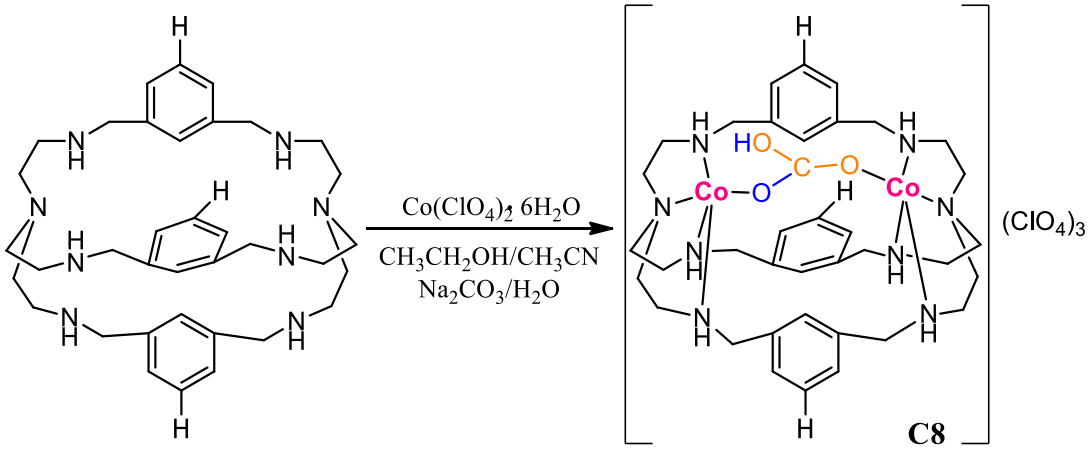

Scheme 2.12 – Synthesis of the cryptate **C8**.

2.3 Compounds characterisation

The characterisation of the different compounds was accomplished using several techniques such as EA, FTIR and NMR: ^{1}H, COSY, ^{13}C-APT, HMQC and HMBC. The ligands **L1** and **L2** were analysed by NMR, the **L2** cannot be compared to the respective complexes **C1** and **C2**, by FTIR, because this ligand is extremely hygroscopic and the KBr pallet were not successfully obtained and the data collected. The four complexes **C1-C4** of Ni(II) and Co(II) were not analysed by NMR as they are paramagnetic compounds and the NMR technique is more suitable for diamagnetic compounds. They were analysed by FTIR.

Elemental analysis for percentage of nitrogen, carbon and hydrogen atoms was performed at C.A.C.T.I. at the University of Vigo. The values obtained were adjusted with solvent molecules and the differences between the calculate and experimental values were ±0.4% (see **Chapter 6-Experimental**). Furthermore, high-resolution mass spectrometry will be performed for a more complete characterisation of the complexes.

2.3.1 Nuclear magnetic resonance (NMR)

2.3.1.1 Characterisation of ligand L1

This characterisation technique was used to identify **L1** and **L2**. **Figure 2.2** allows comparison of the ^{1}H NMR spectra between **E** (red) and **L1** (blue). Here, it is possible to see a small shift of the protons signals that could indicate that the reaction occurred. Another feature is the appearance of new protons signals in the aliphatic group's region present between amine functions ($\mathbf{H_I}$, $\mathbf{H_K}$ and $\mathbf{H_J}$). Additionally, in the aromatic protons region, appears a doublet signal ($\mathbf{H_D}$) confirms that the molecule is asymmetric.

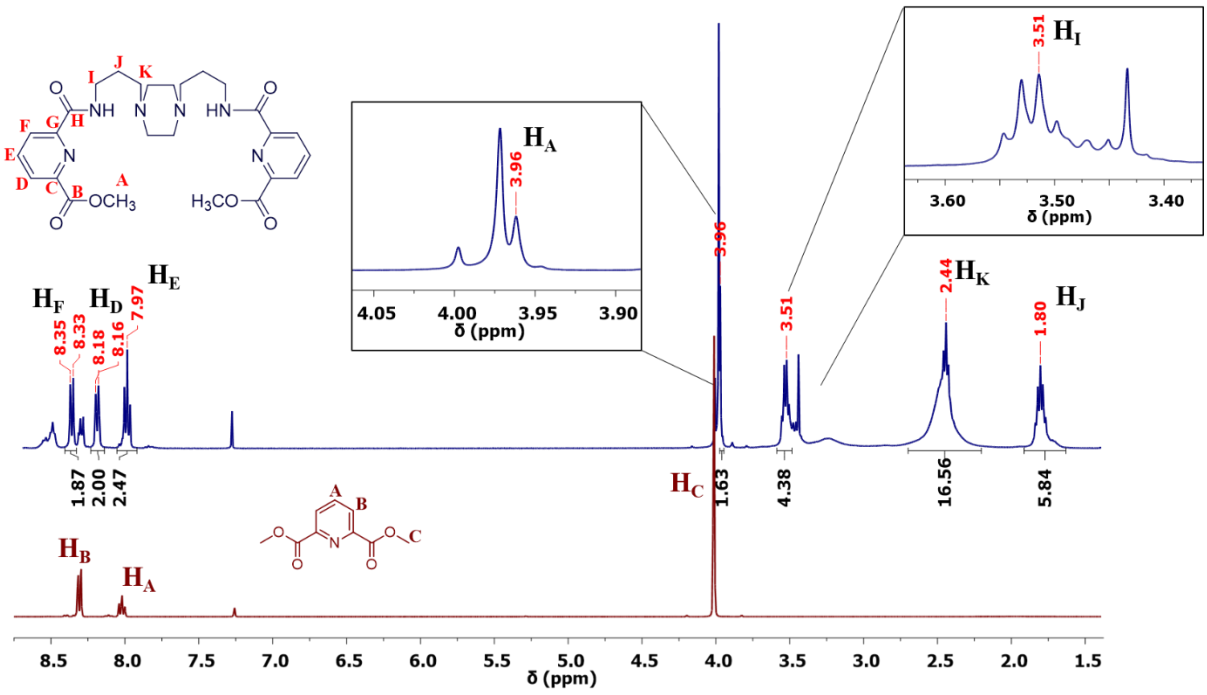

Figure 2.2 – Comparison of ^{1}H NMR spectra **E** (red) and **L1** (blue).

In **Figure 2.2**, it is possible to observe the peaks corresponding to the proton signals of **L1**. Although the spectrum shows some impurities, these did not interfere with the next step of the synthesis. The signals with the chemical shift (δ/ppm) 8.34 ($\mathbf{H_F}$), 8.17 ($\mathbf{H_D}$) and 7.97 ($\mathbf{H_E}$) in the aromatic proton signals

range have an integration value of 2:2:2 and a multiplicity of doublet, doublet and triplet, respectively, as was expected for the pyridyl ring. In the aliphatic protons region, there are signals with the chemical shift (δ/ppm) of 3.96 (**H_A**), 3.51 (**H_I**), 2.44 (**H_K**) and 1.80 (**H_J**). The integration values for these proton signals is different from the expected, but this is possibly due to the presence of impurities. Nevertheless, the elemental analysis results ascertained to the compound formulation (see in **Chapter 6- Experimental**).

The analysis of the ^{13}C-APT NMR (**Figure 8.1** in **Chapter 8 – Annexes**) with the 2D HMQC NMR (**Figure 2.3**) spectra for **L1** allowed to match the protons with their respective carbon signal.

The carbon signals attributed have the chemical shift (δ/ppm) 164.97 (**C_B**), 163.54 (**C_H**), 150.52 (**C_G**), 146.48 (**C_C**), 138.45 (**C_E**), 127.14 (**C_D**), 125.46 (**C_F**), 56.29 (**C_K**), 52.89 (**C_A**), 38.34 (**C_I**), 26.42 (**C_J**).

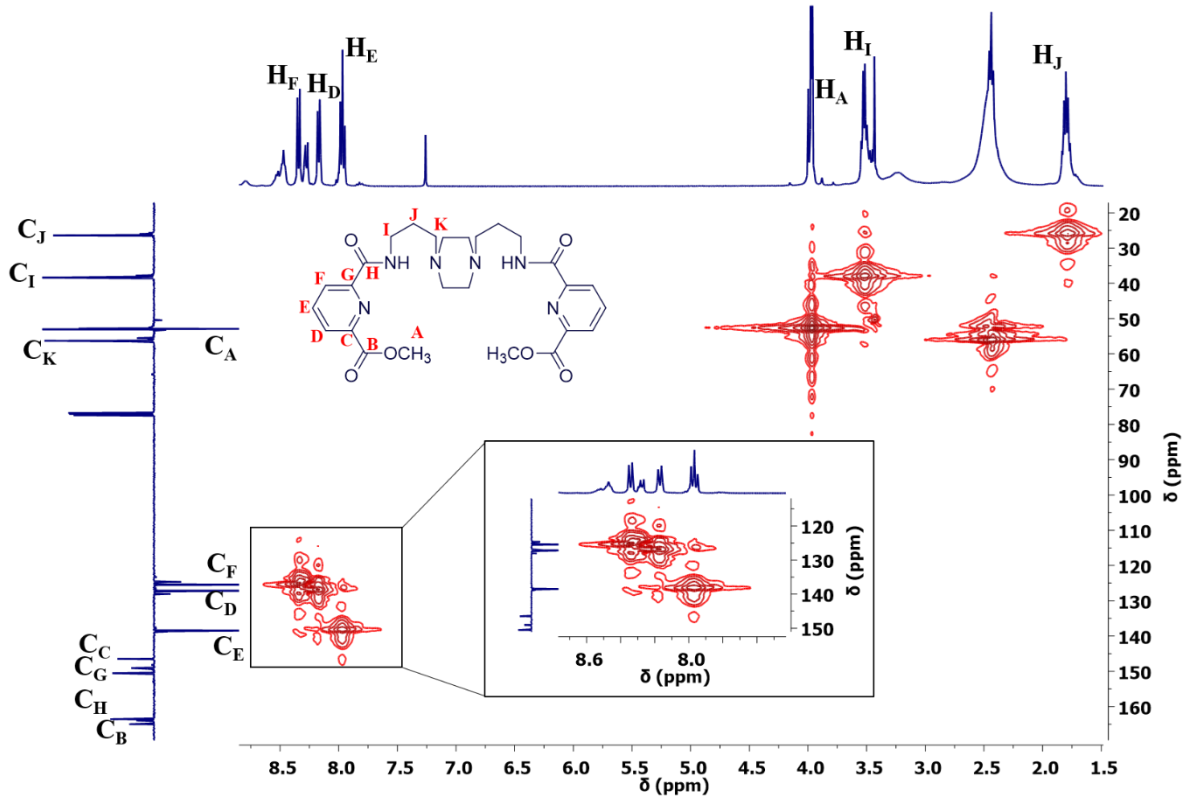

Figure 2.3 – HMQC NMR spectrum of the **L1**, in $CDCl_3$.

The **L1** 2D HMBC NMR spectrum (**Figure 2.4)** was crucial for the identification of all proton/carbon signals of the molecule. Considering that (**H_A)** proton signal at 3.96 ppm have just one correlation to a quaternary carbon signal at 164.97 ppm, it is possible to confirm that the latter signal is from **C_B**. This is confirmed as this carbon (**C_B**) has correlations with the protons signals at 8.17 ppm (**H_D)** and 7.97 ppm (**H_E).** Then, three quaternary carbons remain unidentified and among these three the only quaternary carbon which has a correlation with an aliphatic proton signal (**H_I** at 3.51 ppm) is **C_H** at 163.54 ppm. Additionally, **C_H** has also a correlation with proton signal **H_F** at 8.34 ppm, corroborating the carbon assignment. The remaining two quaternary carbons are **C_G** at 150.52 ppm and **C_C** at 146.48 ppm. These are assigned by exclusion, as **C_G** just show one correlation with the proton **H_E** and the **C_C** carbon have a correlation with the **H_D** and **H_E**.

In the aliphatic region, HMBC NMR spectrum (**Figure 2.4**) permitted to understand that the proton at 3.51 ppm has a correlation with the carbons signals at 26.42 ppm (**C_J)** and 56.29 ppm (**C_K**) and as already mentioned for the carbon signal **C_H**, and for that reason was attributed as **H_I**. The proton signal

at 2.44 ppm, $\mathbf{H_K}$, have a correlation with the carbon signals $\mathbf{C_J}$ and $\mathbf{C_I}$ at 38.34 ppm. Finally, the proton signal at 1.80 ppm $\mathbf{H_J}$ has a correlation to both $\mathbf{C_I}$ and $\mathbf{C_K}$.

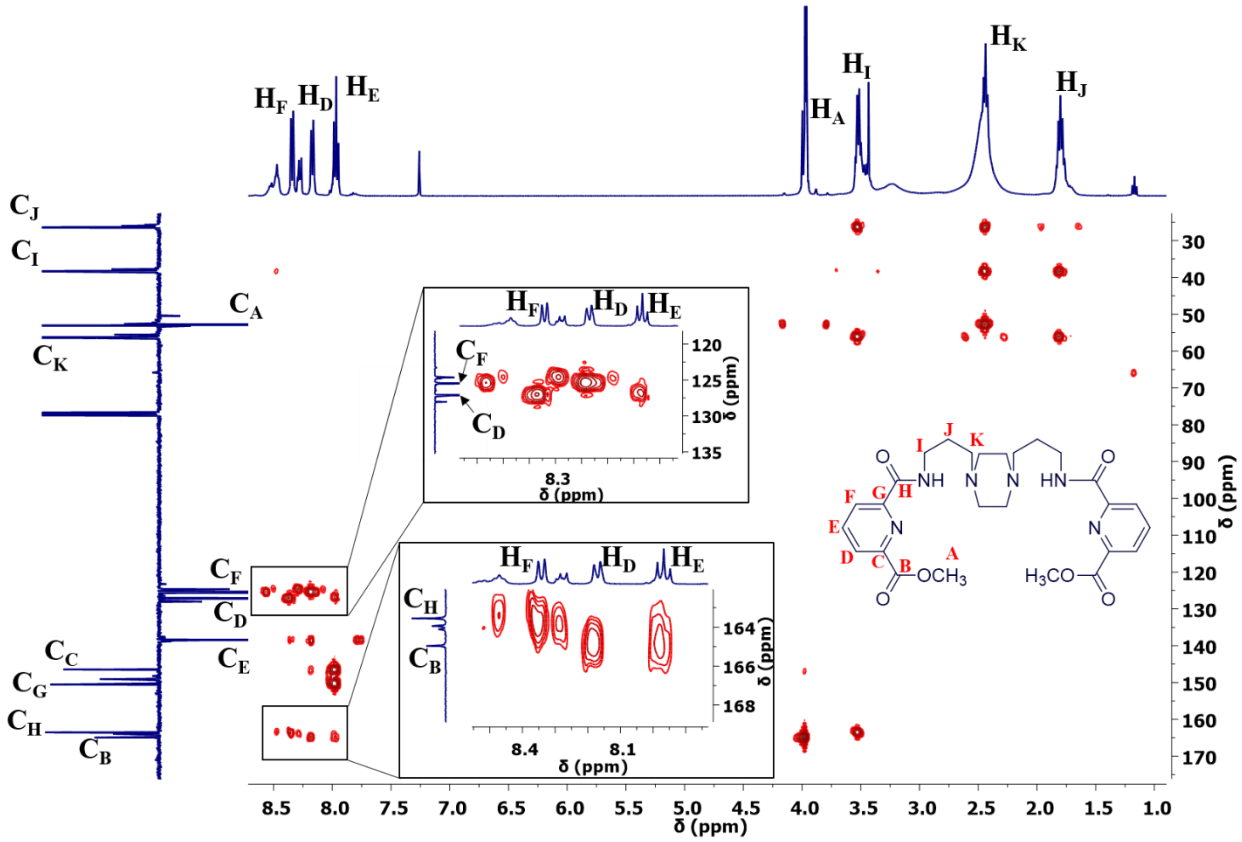

Figure 2.4 – L1 2D HMBC NMR spectrum, in $CDCl_3$.

The protons $\mathbf{H_I}$, $\mathbf{H_K}$, $\mathbf{H_J}$ were attributed by HMBC NMR and the 2D COSY NMR spectrum (**Figure 8.2** in **Chapter 8 – Annexes**) was useful to confirm the assignment of these protons because allowed visualising that the proton signal at 1.80 ppm ($\mathbf{H_J}$) couples with the proton signal $\mathbf{H_I}$ and $\mathbf{H_K}$.

2.3.1.2 Characterisation of L2

In **Figure 2.5** is the ^{1}H NMR spectrum of **L2** and all spectra were analysed analogously as for **L1** (**Figure 8.5-Figure 8.8** in **Chapter 8 – Annexes**). The ^{1}H NMR spectrum shows some impurities that could explain that the integration of the aliphatic proton signals was different from the expected. The analysis of the aromatic protons signal region shows that the pyridine ring is symmetrical as there are just two proton signals at 8.28 and 7.99 ppm with an integration of 4:2, suggesting the macrocycle formation. In the aliphatic proton region, the proton with a chemical shift of 3.09 ppm is the proton signal of the NH function (this signal does not have a corresponding carbon signal, see **Figure 8.7** in **Chapter 8 – Annexes**).

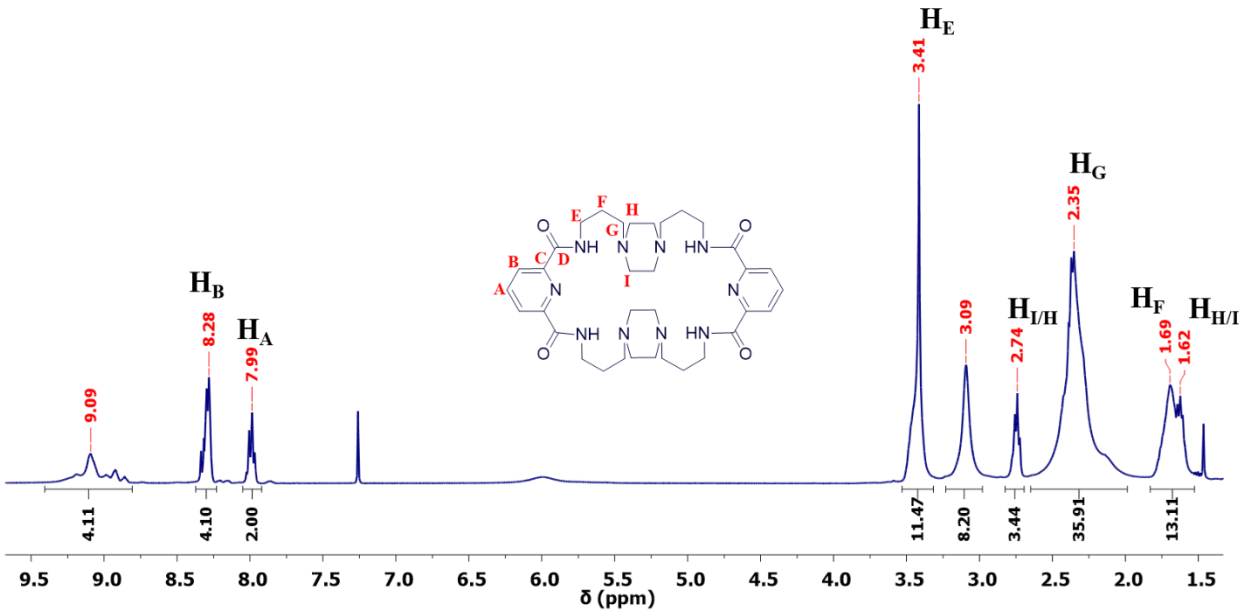

Figure 2.5 – ^{1}H-NMR spectrum of ligand **L2**, in $CDCl_3$.

2.3.1 *Fourier*-transform infrared spectroscopy (FTIR)

The FTIR spectra of the complexes **C1** and **C2** is exhibited in **Figure 2.6**, the more relevant vibrational bands are shown in **Table 2.1**. According to literature[46] the secondary amides in solid state display a band in the region of 1570-1515 cm^{-1}, as result of the N–H group bending (δ_{N-H}). In both spectra there is a δ_{N-H} bending at 1541 cm^{-1}. In the literature[47], the C=O stretching ($\upsilon_{C=O}$) vibration mode for amides appears below 1700 cm^{-1} and does not reach 1600 cm^{-1}. The complexes **C1** and **C2** show this band at 1632 and 1664 cm^{-1} respectively. The counter anion (perchlorate) vibrational modes appear at 1088 and 624 cm^{-1} for both complexes.

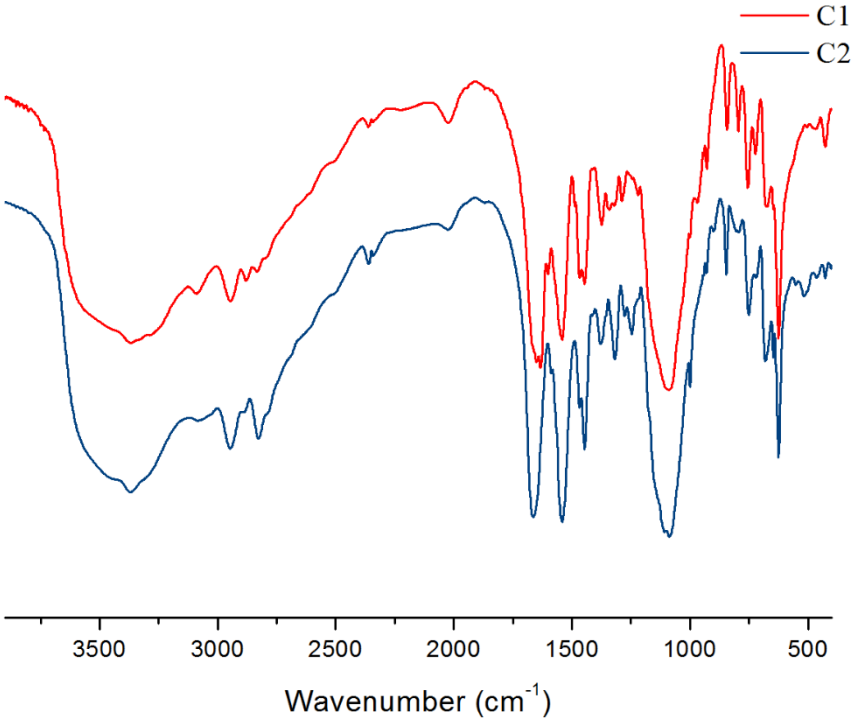

Figure 2.6 – FTIR spectra of the complexes **C1** (red) and **C2** (blue).

Table 2.1 – Wavenumber of characteristic bands, $\bar{\nu}$(cm^{-1}), of the complexes **C1-C4**.

	Wavenumber (cm^{-1})						
Complexes	ν_{CH_2}	ν_{N-H}	$\nu_{C=O\ (amide)}$	δ_{N-H}	ν_{CO_3H}	$\nu_{ClO_4^-}$	
C1	2945 2879 2833	3365	1632	1541	-	1088	625
C2	2951 2827	3371	1664	1541	-	1088	625
C3	2917 2877	3273	-	-	1672	1090	625
C4	2924 2876	3267	-	-	1635	1090	625

The spectra of **L6** and **C4** are depicted in **Figure 2.7** (**C3** can be seen in **Figure 8.9** in **Chapter 8 – Annexes**). According to literature[16] two peaks corresponding to the vibrational modes of the counter anion perchlorate emerge at values between 1018-1122 cm^{-1} and 621-626 cm^{-1}. For both complexes, the values observed were 1089 and 624 cm^{-1}. The band corresponding to HCO_3^- vibrational mode could be found at 1672 cm^{-1} for **C3** and at 1635 cm^{-1} for **C4**.

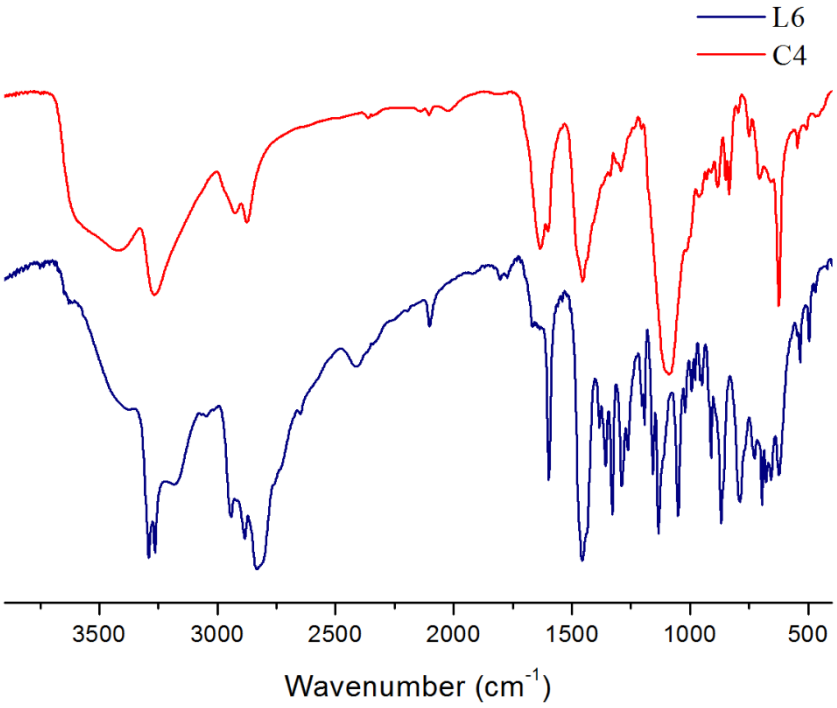

Figure 2.7 – FTIR spectra of the cryptand **L6** (blue) and cryptate **C4** (red).

Chapter 3

Complex immobilisation on multi-walled carbon nanotubes

3. Complex immobilisation on multi-walled carbon nanotubes

This chapter addresses the covalent immobilisation of **C3** (due to the lack of time the **C4** do not was used for the covalent immobilisation). This complex has a C≡CH function that allows its covalent immobilisation on multi-walled carbon nanotubes (MWCNT). The MWCNT were modified using a diazonium salt, the 4-[(trimethylsilyl)ethynyl]benzene diazonium tetrafluoroborate. It was prepared in two steps, based on a procedure from literature.[48,49] In **Scheme 3.1** are represented the reactions performed for **C3** immobilisation on MWCNT. The first step of the modification was the graffitiing of 4-[(trimethylsilyl)ethynyl]benzene on MWCNT surface (**CNT1**). After, the deprotection of the triple bond by removing the trimethylsilyl group using tetrabuthylammonium fluoride was accomplished (**CNT2**). The complex attachment is done by Glaser coupling between two triple bonds present on both the complex and **CNT2 (CNT3**, **Scheme 3.1)**.[50]

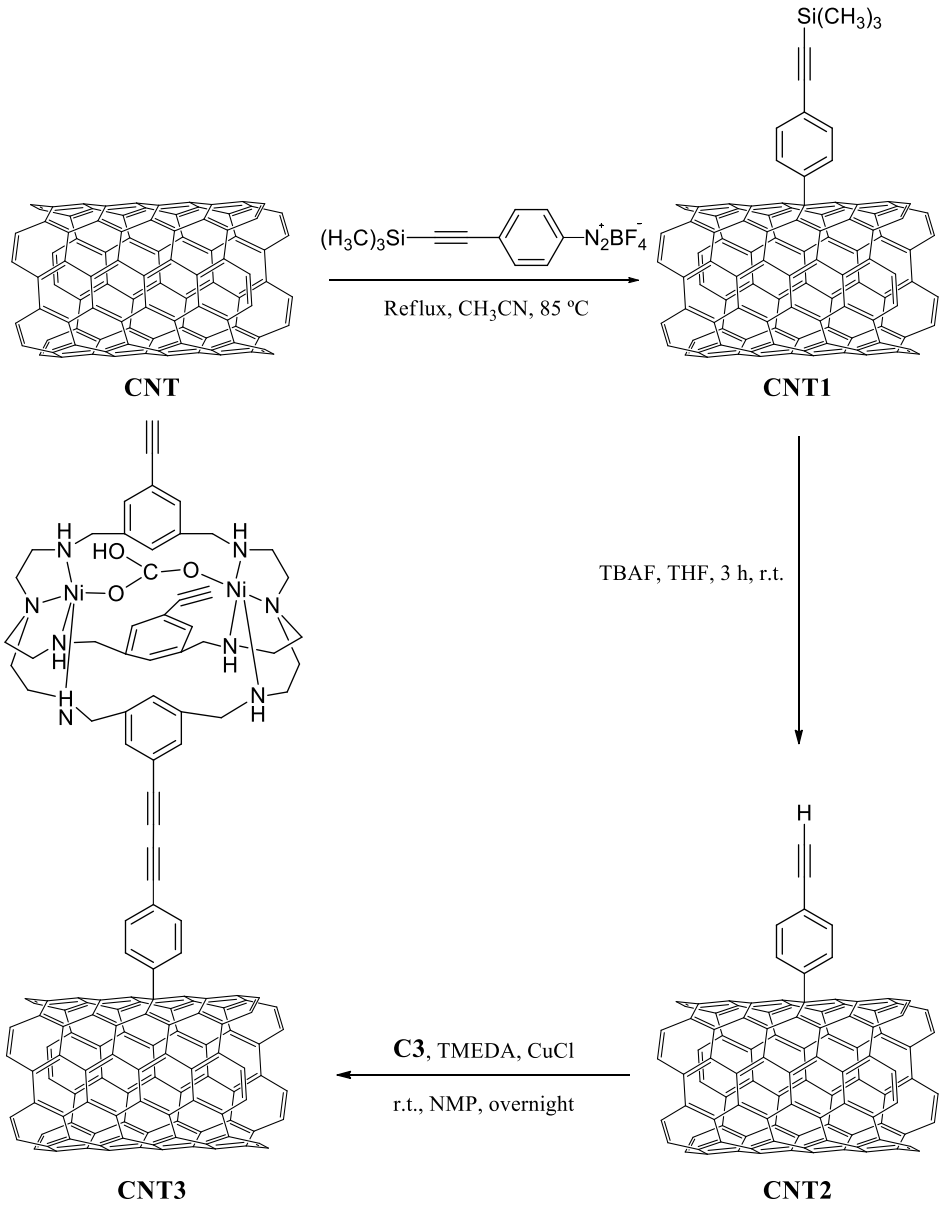

Scheme 3.1 – Synthetic procedure for **C3** covalent immobilisation on MWCNT.

3.1 Characterisation of the modified MWCNT

The pristine MWCNT and the new modified MWCNT (**CNT1**, **CNT2** and **CNT3**) were characterised by atomic absorption spectroscopy (AAS) and X-ray photoelectron spectroscopy (XPS). The AAS studies were performed by Dr. Ana Mourato from Faculdade de Ciências da Universidade de Lisboa and XPS analysis by Professor Ana Maria Rego from Instituto Superior Técnico da Universidade de Lisboa.

3.1.1 Atomic absorption spectroscopy (AAS)

Preliminaries qualitative studies of atomic absorption spectroscopy were performed to understand if the immobilisation occurred. The characterisation of the pristine and modified MWCNT by AAS was performed for two different analytes: copper and nickel (**Table 3.1**). The samples were prepared on different days which results on different calibration curves for each sample interfering in the results obtained. Although mg/kg values were determined, these results are mostly qualitative as to have a quantitative analysis more than one repetition is necessary. Therefore, only the qualitative analysis of analyte variation with MWCNT modification steps will be discussed.

Table 3.1 – Ni and Cu amount detected in pristine and modified MWCNT by AAS.

		Analyte amount (mg/kg)	
Entry	Samples	Cu	Ni
1	**CNT**	36	708
2	**CNT1**	0	263
3	**CNT2**	260	327
4	**CNT3**	54735	2756

Entry 1 represents the analytes detected on MWCNT (**CNT** in **Scheme 3.1**). The non-existence of copper in **Entry 2** is not in agreement with the remaining results what could indicate an outlier as the MWCNT already have copper in their composition. The results from **Entry 3** to **Entry 4** show an increase of the amount of copper that can be explained by the **CNT3** synthesis procedure that uses copper chloride as catalyst. As expected the amount of nickel increases considerably in **Entry 4**, suggesting the immobilisation of the Ni(II) cryptate (**C3**) on the MWCNT.

3.1.2 X-ray photoelectron spectroscopy (XPS)

The XPS characterisation was accomplished for Si 2p, O 1s, N 1s, Ni 2p and Cu 2p regions in **CNT1-3**. The spectra are shown in **Figure 3.1**, indicates that the cryptate **C3** was immobilised on MWCNT. The C 1s region analysis was not included in the XPS discussion since in this system, carbon results are not very informative.

In the spectrum for **CNT1**, a feature at 102 eV corresponding to the Si 2p region (**Figure 3.1(a)**) is observed, which is consistent with the presence of the trimethylsilyl group. It is possible to fit two peaks corresponding to Si $2p_{3/2}$ and Si $2p_{1/2}$ at 102.2 and 101.8 eV, respectively.[51] This signal is not observed in the **CNT2** spectrum as this material is obtained from the triple bond deprotection reaction on **CNT1** that removes the silyl group. As expected, **CNT3** does not have any feature in that region. Another important region is the O 1s region at 532 eV (**Figure 3.1(b)**) where a signal is observed for all three samples, however with higher intensity for **CNT3**. Additionally, for **CNT3** two peaks could be fitted at 532.5 eV, corresponding to the oxygens from the carbonate, $C\underline{O}_3$ and at 534.9 eV possibly corresponding to $H_2\underline{O}$ bonds.[52,53] This was expected as a carbonate molecule is present in **C3** that was immobilised on

MWCNT yielding **CNT3**. For the N 1s region (**Figure 3.1(c)**) a feature at 399.8 eV is detected which is consistent with the presence of C-N group[54] from the amine functions on **C3**. As expected, signals at the Ni 2p region (between 870-855 eV) (**Figure 3.1(d)**) were only found for **CNT3** after complex immobilisation. At 856.7 eV is the Ni $2p_{3/2}$ and three multiplet signals between 862.5-868.8 eV. The binding energies at 856.7 eV for Ni 2p3/2 are spin-orbit characteristics of Ni(II) in oxide, hydroxide and organometallic compounds.[55] The Cu 2p region (peaks at 935 and 945 eV) (**Figure 3.1(e)**) was also analysed as copper was used as catalyst in the **C3** immobilisation reaction. The peak at 935.5 eV corresponds to Cu $2p_{3/2}$ and the existence of multiplet peaks in the spectra suggest that the copper present in the samples is Cu(II).[56] As shown by AAS, the quantity of Cu(II) in the sample is higher than the Ni(II) one.

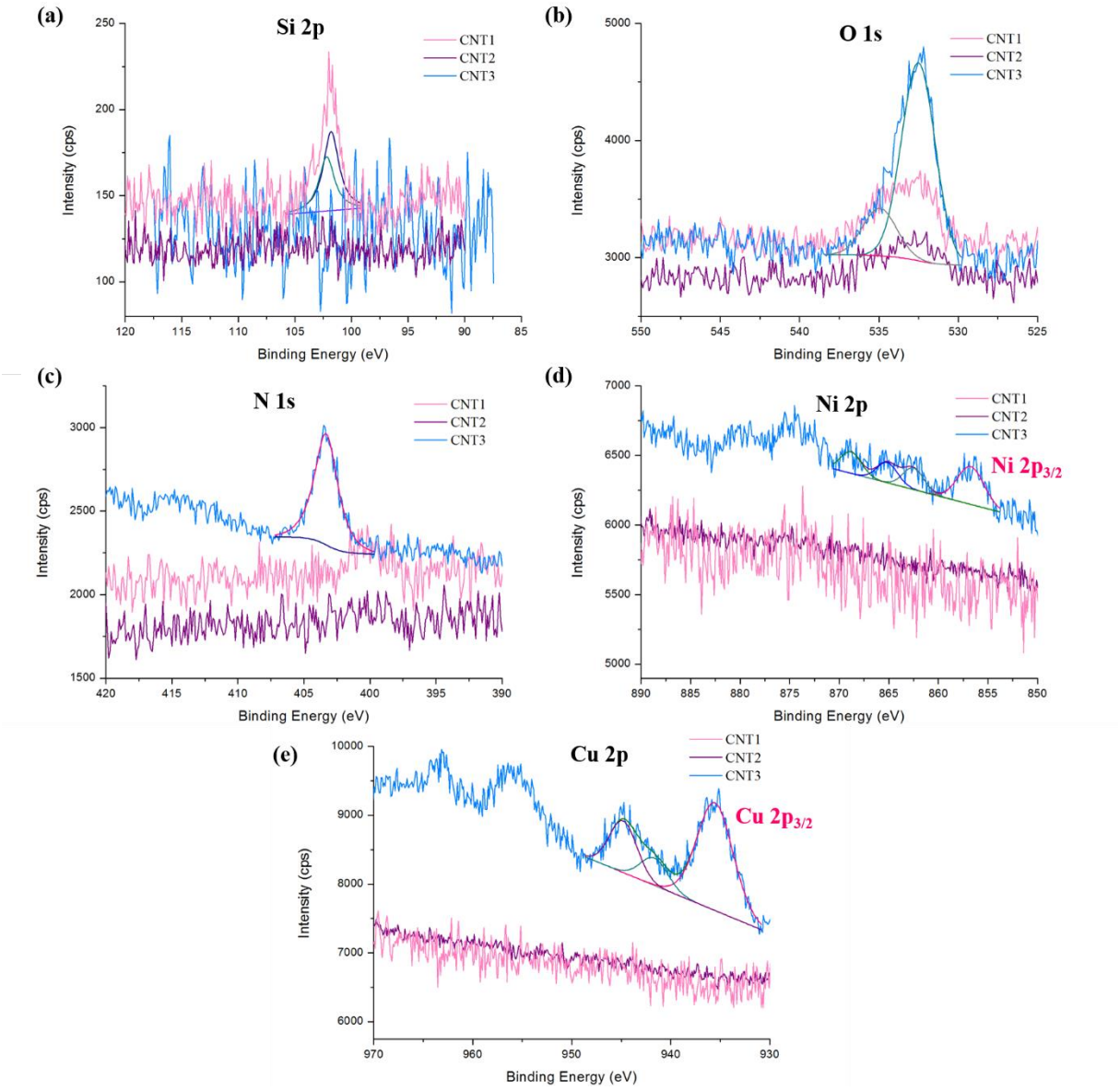

Figure 3.1 – XPS spectra of **CNT1-3** Si 2p, O 1s, N 1s, Ni 2p and Cu 2p regions.

This characterisation technique was also used to determine the atomic percentages of the elements on **CNT3** (**Table 3.2**). The ratio N/Ni should be 4 (8/2), however the ratio obtained was 6.01 and this can be explained as the nickel(II) signal is low and the associated error in the area estimation can interfere on this result.

Table 3.2 – Atomic percentage (%) determined by XPS for **CNT3**.

	Atomic %	Ratio N/Ni
N 1s	24.01	6.01
O 1s	55.13	
Ni 2p	4.00	
Cu 2p	16.86	

Chapter 4

CO_2 photoreduction studies

4. CO_2 photoreduction studies

CO_2 photoreduction studies were performed using Ni(II) and Co(II) complexes **C1-C8** as catalysts (**Figure 4.1**). Two different set-ups were used and for both a 5 mL solution (v/v= 4:1 CH_3CN/H_2O), $[Ru(phen)_3](PF_6)_2$ as photosensitiser (PS) and triethanolamine (TEOA) as sacrificial donor (SD) were employed. A heterogeneous CO_2 photoreduction experiment was performed using **CNT3** as catalyst.

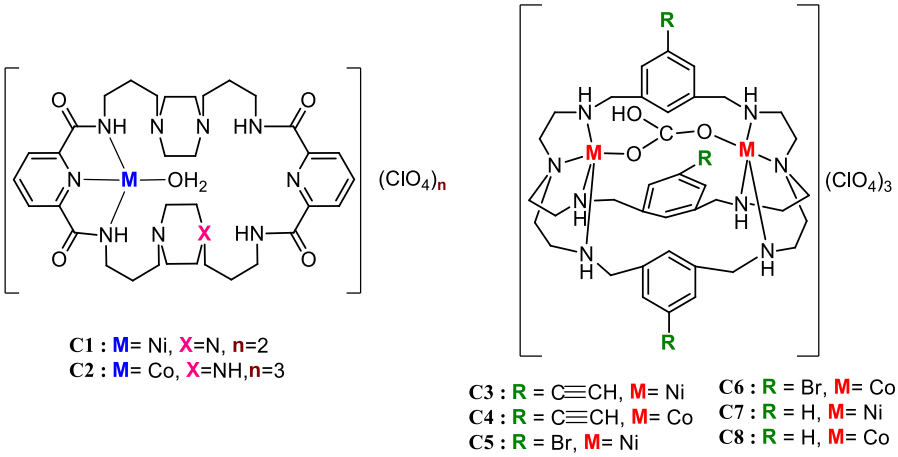

Figure 4.1 – Complexes used on CO_2 photoreduction studies.

Set-up I was composed by a box with a magnetic stirrer, an support for the reactor, three blue LED lights sources (λ= 492-455 nm) and the experiments were carried out for 6 h (**Figure 4.2** on the left). On the other hand, the **set-up II** with a solar light simulator (λ= 400-750 nm **Figure 8.10** in **Chapter 8 – Annexes**) an experiment time of 72 h (**Figure 4.2** on the right). The difference on the experiment time between both set-ups is related with the energetic power of both lights. Different PS/SD systems were also investigated such as purpurin/triethylamine (TEA), 9-antracenecarbonitrile/TEA, purpurin/BIH, $[Ru(phen)_3]_2(PF_6)_2$/BIH/TEOA, however the results did not reveal any gaseous CO_2 reduction product.

Figure 4.2 – Illustrative figure of the inside of the **set-up I** (blue LED light, left) and **set-up II** (solar light simulator, right).

The CO_2 photoreduction ability of the different catalysts used was explored and compared. To analyse the headspace gases produced a GC-TCD was used (for details see **Chapter 6 – Experimental**) and the liquid phase was first analysed by ionic chromatography without success. For a qualitative evaluation of the presence of liquid CO_2 reduction products, a ^1H NMR method based on literature[57] was also performed.

All the experiments were performed with 2 μM of catalyst. The experiments should have been carried out at least 3 times each but due to lack of time that was not possible. The results obtained for the **set-up I** are shown in **Table 4.1** and for **set-up II** in **Table 4.2**. TON and TOF values were higher for **C6** and **C2** complexes and lowest values were obtained for **C1**. All cobalt complexes in this set-up, showed better results for TON_{CO}, TOF_{CO} and Φ_{CO} (equation (1)) when compared to the nickel complexes. The

selectivity for CO was higher for **C3** (97%) and the lowest result was produced by **C1** (84%). In general, all complexes showed good values of selectivity (≥84) for this set-up.

$$\Phi_{CO} = \frac{moles\ of\ products \times 6.022\times10^{23} \times 2}{incident\ number\ of\ photons} \times 100\% \qquad (1)$$

Table 4.1 – CO_2 photoreduction results, for the **set-up I**, with 6 h experiments.*

Catalyst (2 µM)	n_{CO} (µmol)	n_{H_2} (µmol)	$CO_{select.}$ (%)	TON_{CO}	TOF_{CO} (h^{-1})	Φ_{CO} (%)
C1	1.28	0.07	95	128	21	0.183
C2	11.4	1.26	90	1138	190	1.631
C3	3.18	0.10	97	318	53	0.455
C4	7.27	1.06	87	727	121	1.042
C5	2.80	1.08	96	280	47	0.402
C6	13.36	1.75	88	1336	223	1.915
C7	1.71	0.136	93	170	28	0.244
C8	3.47	0.68	84	347	58	0.497
Without cat.	0	0	0	0	0	0

*Reaction conditions: 4 mL CH_3CN: 1 mL H_2O, $Ru(phen)_3(PF_6)_2$ (0.4 mM), TEOA (0.3 M), LED light (Dimmable Blue LED Spot Light Bulb, 15 W), 6 h experiments, 3.89×10^{16} photons per second calculated for this set-up using $K_3[Fe(C_2O_4)_3]$ actinometer (**Chapter 6 – Experimental**).

The results for **set-up II**, in a similar fashion as for **set-up I**, showed that the complexes with higher TON and TOF values are the cobalt complexes with exception of **C3**. Once again, the higher TON_{CO} value is verified for **C6** and **C2**, and the lowest value for **C7**. The selectivity values were higher for **C3** and **C5** (97%) and extremely low for **C6** (20%). This selectivity value for **C6** (20%) is due to the presence of methane in the gaseous headspace. This catalyst was the only one that showed the presence of methane (**Table 4.3**) and a deeper investigation is needed to verify if the remaining catalysts can also produce this gas.

Table 4.2 – CO_2 photoreduction results, for **set-up II**, 72 h experiments.*

Catalyst (2 µM)	n_{CO} (µmol)	n_{H_2} (µmol)	n_{CH_4} (µmol)	$CO_{select.}$ (%)	TON_{CO}	TOF_{CO} (h^{-1})	Φ_{CO} (%)
C1	3.12	0.32	-	91	312	4	0.116
C2	7.54	0.91	-	43	754	10	0.281
C3	5.22	0.16	-	97	523	7	0.195
C4	7.27	1.06	-	86	546	8	0.204
C5	4.24	0.14	-	97	424	6	0.158
C6	8.02	31.80	0.50	20	802	11	0.299
C7	2.72	0.35	-	89	272	4	0.102
C8	5.09	4.2	-	55	509	7	0.190
Without cat.	0	0		0	0	0	0

*Reaction conditions: 4 mL CH_3CN: 1 mL H_2O, $Ru(phen)_3(PF_6)_2$ (0.4 mM), TEOA (0.3 M), solar light simulator lamp (Projection lamp, 150 W), 72 h experiments, 1.2457×10^{16} photons per second calculated for this set-up using $K_3[Fe(C_2O_4)_3]$ actinometer (**Chapter 6 – Experimental**).

Table 4.3 – CO_2 photoreduction result of methane.

	n_{CH_4} (µmol)	$CH_{4_{select.}}$ (%)	TON_{CH_4}	TOF_{CH_4} (h^{-1})	Φ_{CH_4} (%)
C6	0.50	1	50	0.69	0.02

In conclusion, the cryptate substituent influences the TON_{CO} and TOF_{CO} values. For the cobalt complexes a deactivating group (bromide) yields higher values than when an activating group (C≡CH) is present. In opposition, for the nickel complexes an activating group (C≡CH) produced better results than when the deactivating group (bromide) was present. For the pincer macrocycle complexes the results were similar since the cobalt complex (**C2**) shows better TON_{CO}, TOF_{CO} and Φ_{CO} values than the Ni complex (**C1**).

In addition to gaseous products, the CO_2 photoreduction experiments can originate in liquid phase products, such as formic acid, formaldehyde, among others. To detect whether formic acid is present, an extraction from the liquid phase with D_2O and CH_2Cl_2 was performed. To 2 mL of the solution after 6/72 h of photoirradiation was added 0.8 mL of D_2O and after 5 mL of CH_2Cl_2 was combined creating a biphasic solution. The aqueous phase was transferred to an NMR tube and one drop of concentrated HCl was added.

In **Figure 4.3** is represented the region of the proton shift corresponding to the formic acid proton (HCOOH). This analysis corresponds to **C4** liquid products from **set-up II**. This test was performed for almost all the photoreduction samples and the results are in **Table 4.4**. The remaining the samples were not studied due to lack of time.

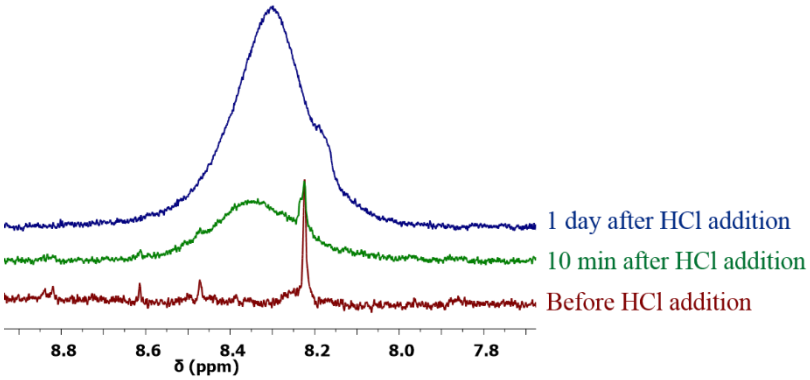

Figure 4.3 – ^1H NMR spectra of the liquid phase when **C4** used as catalyst after photoirradiation for 72 h. Before the addition of a drop of HCl in red, 10 min after the addition in green and 1 day after the addition in blue.

Table 4.4 – Qualitative determination of formic acid in CO_2 photoreduction experiments by ^1H NMR.

Catalysts	**Set-up I**	**Set -up II**
C1	yes	no
C2	no	no
C3	no	no
C4	no	yes
C5	no	-
C6	no	no
C7	-	-
C8	-	-

* The test was not performed in the samples **C7**, **C8** for both set-ups and for sample **C5** set-up II.

A heterogeneous CO_2 photoreduction experiment was performed using **CNT3** as catalyst, for set-up I, with reaction conditions based on the literature.[58] The experiment was composed of 2.0 μM of $[Ru(phen)_3](PF_6)_2$, 0.5 M of TEA and 2 mg of **CNT3** in an acetonitrile solution with 5% of H_2O. 2 mg of the **CNT3** correspond to approximately 8 μM of Ni(II) calculated using the AAS values obtained for **CNT3**. However, the gaseous phase was analysed by GC-TCD and only showed H_2 as by-product and no CO_2 photoreduction products were observed. Thus, further studies are still needed, with different amounts of catalyst, different systems of PS/SD and solvents.

Further studies should be carried out to verify the efficiency and durability of the catalysts, such as studies with different concentrations of catalyst and experiments with longer irradiation times.

Chapter 5
Conclusions

5. Conclusions

In this thesis two different types of ligands were synthesised: a macrocycle containing an NNN-pincer moiety and octaazacryptands. These ligands were used to coordinate Ni(II) and Co(II). All compounds were successfully obtained and identified by several characterisation techniques (NMR, FTIR, EA). The Ni(II) and Co(II) complexes were used as catalysts for carbon dioxide photoreduction studies.

To assure that the by-product [1+1] macrocycle was not obtained, first an open-chain ligand was isolated ([2+1] product) and only afterwards reacted it with the desired amine.

For the octaazacryptates, three different ligands were used to synthesise the complexes by changing the substituents on the aromatic rings. Thus, one was modified with an electron withdrawing group (Br), the second was composed by an electron-donating substituent (C≡CH) and the third without any substituent.

The CO_2 photoreduction studies were performed in homogeneous medium using two different set-ups. One was composed by a three blue LED light source (λ= 492-455 nm) and the other was based on a solar light simulator (λ= 400-750 nm). Experiments were performed with different pairs of photosensitiser/sacrificial donor, however only one of these showed the ability to reduce CO_2. To analyse the headspace gaseous products a GC-TCD was used and the liquid phase was first analysed by ionic chromatography, however without success. As an alternative, a qualitative evaluation of the presence of liquid CO_2 reduction products was carried out by a ^{1}H NMR method based on literature procedures and formic acid was detected for only two of the analysed samples.

The macrocyclic complexes containing the NNN-pincer moiety revealed that the cobalt(II) complex produced better TON_{CO} and TOF_{CO} values than the nickel(II) complex with both set-ups. For both set-ups, the CO_2 photoreduction showed better results for the cobalt(II) cryptate with the electron withdrawing group (Br). In opposition, for the nickel(II) cryptates the best results were observed when an electron-donating substituent (C≡CH) was present. In general, all cobalt(II) complexes showed better results than the nickel(II) complexes.

A covalent immobilisation of a Ni(II) cryptate on carbon nanotubes was accomplished. The characterisation techniques (AAS and XPS) revealed that the immobilisation occurred, however large amounts of copper(II) in the material were detected. This is due to the use of Cu(I) as a catalyst in the last step of the complex immobilisation. Afterwards, a heterogeneous CO_2 photoreduction experiment was performed using the modified carbon nanotubes as catalyst. The gaseous phase was analysed by GC-TCD and only showed H_2 as by-product and no CO_2 photoreduction products were observed. Thus, further studies are still needed, with different amounts of catalyst, different systems of PS/SD and solvents.

Chapter 6
Experimental

6. Experimental

In this chapter the reagents, instrumentation and methods used, as well as, the synthesis of the compounds and their characterisation spectra will be described.

6.1 Reagents

The reagents used were isophthalaldehyde ($C_8H_6O_2$,TCI Chemicals, >98%), N-bromosuccinimide ($C_4H_4BrNO_2$, Acros Organics, 99%), tris(2-aminoethyl)amine ($C_6H_{18}N_4$,TCI Chemicals, >98%), sodium cyanoborohydride ($NaBH_3CN$, Acros organics, 95%), cobalt(II) perchlorate hexahydrate ($Co(ClO_4)_2{\cdot}6H_2O$, Alfa Aesar), nickel(II) perchlorate hexahydrate ($Ni(ClO_4)_2{\cdot}6H_2O$, Alfa Aesar), iron(III) chloride ($FeCl_3$, Merck, >98%), potassium oxalate ($C_2K_2O_4$, Merck), 2,6-pyridinedicarboxylic acid ($C_7H_5NO_4$, Acros Organics, 99%), 1,4-bis(3-aminopropyl)piperazine ($C_{10}H_{24}N_4$, Alfa Aesar, 98%), ruthenium(III) chloride hydrate (Precious metals online), 1,10-phenantroline monohydrate ($C_{12}H_8N_2{\cdot}H_2O$, TCI Chemicals, 99%), sodium carbonate (Na_2CO_3, Bronalab), carbon nanotubes multi-walled (>98% carbon basis, O.D. × L 6-13 nm × 2.5-20 μm, Aldrich), Purpurin ($C_{14}H_8O_5$, Acros Organics), 9-antracene carbonitrile ($C_{15}H_9N$, Alfa Aesar, 98%),acetic acid (CH_3COOH, Merck, 96%), sulfuric acid (H_2SO_4, Panreac, 98%), nitric acid fuming (HNO_3, Carlo Erba, 90%), sodium hydroxide PA lentils (NaOH, Eka Chemicals). No previous purification was performed before use.

6.2 Instrumentation

During this work, different characterisation techniques were carried out. The **NMR** spectra were acquired on a Bruker Advance 400 spectrometer using deuterated solvents. All the peaks were reported having the solvent peak as reference.

FTIR spectra were recorded on a Nicolet Nexus 6700 FTIR spectrophotometer in the 400-4000 cm^{-1} range, resolution 4 cm^{-1} using KBr pellets.

Elemental analysis for nitrogen, carbon and hydrogen atoms, was performed at C.A.C.T.I. in University of Vigo, using an elemental analyser Carlo Erba 1108.

The **CO_2 photoreduction** studies were performed in two different set-ups where the first one included inside of the box, one magnetic stirrer three LED lights (Dimmable Blue LED Spot Light Bulb, 15W) that directly irradiated a glass reactor with a capacity of 11.5 mL. The experiments under CO_2 atmosphere (1 atm) were made with 2 μM of catalyst and different sets PS/SD and solvents:

- 0.4 mM of $[Ru(phen)_3]_2(PF_6)_2$, 0.3 M triethanolamine in 5 mL of acetonitrile/water (v/v 4:1) over 6 h
- 0.4 mM of purpurin, 0.1 M $NaHCO_3$, 50 mM triethylamine in 5 mL of acetonitrile/water (v/v 1:9) over 6 h.
- 0.2 mM of 9-antracene carbonitrile, 0.36 M of triethylamine in 5 mL of acetonitrile over 6h.
- 0.02 mM of purpurin, 0.1 M of BIH in 5 mL of DMF, over 6h.
- 0.3 mM of $[Ru(phen)_3]_2(PF_6)_2$, 0.1 M of BIH, 0.5 M of triethanolamine in 5 mL of acetonitrile, over 6h.

The second set-up contained a solar light lamp (Projection lamp, type 13117, 17V, 150W, GX5.3) directly irradiating the glass reactor with the same capacity of 11.5 mL for 72 h.

The number of irradiated photons per second was determined using a procedure from literature.[59]

The **gas quantification**, a gas chromatograph fitted with a thermal conductivity detector was used from Agilent Technology (GC-TCD 7820A) controlled by OpenLAB ChemStation edition software. A carboxen®-1006 PLOT Capillary GC Column (L ×I.D. 30 m × 0.53 mm, average thickness 30 μm)

was used for H_2, CO and CO_2 detection. The temperature was held at 230 ºC for injector and detector. The carrier gas was argon (Ar) flowing at 3 $mLmin^{-1}$ and injections were performed with a gas-tight syringe (500 µL) previously purged with CO_2. The method used was based on keeping the oven at a constant temperature of 30 ºC.

The retention times (min): H_2 3.304, N_2 3.464, O_2 3.517, CO 3.591, CO_2 7.713. Calibration curves were obtained for H_2 and CO separately by injecting know volumes of pure gas using method described.

The carbon nanotubes characterisation was achieved by **Atomic absorption spectroscopy** on a novAA 350 Flame Atomic Absorption Spectrometer from Analytik Jena. The flame type was carried on air/acetylene with a fuel flow rate of 0.8 to 1.0 l/min for Cu, Co and Ni analysis. The sample preparation was performed in a platinum crucible. Before the deposition of the sample, it was boiling during 1 h with a 1:1 mixture of HCl/H_2O Millipore then was washed with water Millipore and was calcinated in an oven furnace at 750 ºC during 1 h. The sample (10 mg) was calcined for 3 h at 550 ºC in an oven furnace. Then was attacked with 1 mL of aqua regia on a magnetic stirrer at 120 ºC and was transferred to volumetric flask.

X-ray photoelectron spectroscopy (XPS) experiments were performed by Prof Ana Maria Rego from Instituto Superior Técnico. XPS characterisations were run on a XSAM800 (KRATOS) spectrometer in fixed analyser transmission mode, with pass energy of 20 eV and non-monochromatised Mg Kα X-radiation (hυ = 1253.6 eV). Samples were mounted on the sample holder through a double-sided tape by pressing the powder. They were analysed at room temperature and in an ultrahigh vacuum chamber (10^{-7} Pa). The spectra were recorded using Vision 2 software for Windows, Version 2.2.9 and a step of 0.1 eV. Components curves were fitted with pseudo-Voigt profiles (Gaussian-Lorentzian products) with a non-linear minimum square method using a freeware program (XPSPEAK41). The binding energies were were not corrected for charge accumulation since the carbon component with the lowest binding energy (and higher intensity) was centred at 284.9 eV corresponding to a mixture of sp^2 and sp^3 carbons bound to other carbon or hydrogen atoms. For quantification purposes, the sensitivity factors were 0.318 for C 1s, 0.505 for N 1s, 2.337, 0.736 for O 1s, and 3.845 for Ni $2p_{3/2}$.

6.3 Compounds Synthesis

The synthesis of the compounds will be shown in this section.

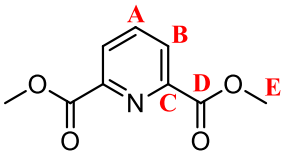

To synthesize the dimethylpyridine 2,6-dicarboxylate a procedure in literature were used.[43] Mass obtained 4.175 g, yield 76 %.

^{1}H NMR (400 MHz, $CDCl_3$, 298 K) δ/ppm: 8.31 (d, J=8.31 Hz, 2H, **H_B**), 8.02 (t, 1H, **H_A**), 4.01 (s, 6H, **H_E**).

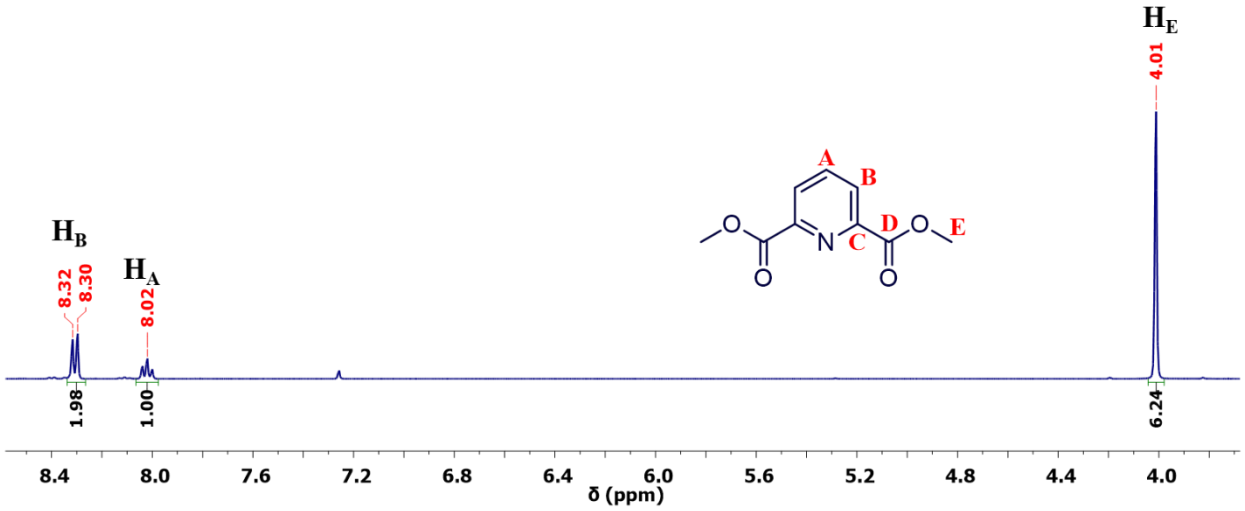

Figure 6.1 – ^{1}H NMR spectrum of **E**, in $CDCl_3$.

6.3.1 Ligands synthesis

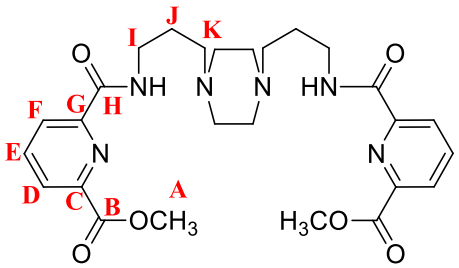

L1

The ligand precursor was prepared by using a modified method from the literature for a similar compound.[44] To avoid the formation of [1+1] condensation product was used 0.27 equivalents of 1,4-Bis(3-aminopropyl)piperazine. The 1,4-Bis(3-aminopropyl)piperazine, 656 µL (3.19 mmol), was dissolved in 10 mL of methanol and was added dropwise (in one hour and a half) to 2.303 g (11.80 mmol) of the dimethyl 2,6-pyridine dicarboxylate dissolved in 20 mL at reflux. The mixture reaction was refluxed overnight and after cooling to room temperature the solvent was evaporated, and a coral paste was obtained.

The crude was recrystallized from hot methanol and left one night in the fridge. A white precipitate was formed and filtered (the remaining ester unreacted). The solvent of the filtrate was evaporated under vacuum and was obtained an oil it was washed multiple times with diethyl ether. The result was a soft coral solid. Mass obtained 1.141 g, yield 68%.

^{1}H NMR (400 MHz, $CDCl_3$, 298 K) δ/ppm: 8.34 (d, J=8.34 Hz, 2H, **H_F**), 8.17 (d, J=8.17 Hz , 2H, **H_D**), 7.97 (t, 2H, **H_E**), 3.96 (s, 6H, **H_A**), 3.51 (d,4H, **H_I**), 2.44 (m, 12H, **H_K**), 1.80 (q, 4H, **H_J**).

^{13}C NMR (100 MHz, $CDCl_3$, 298 K) δ/ppm: 164.97 (**C_B**), 163.54 (**C_H**), 150.52 (**C_G**), 146.48 (**C_C**), 138.45 (**C_E**), 127.14 (**C_D**), 125.46 (**C_F**), 56.29 (**C_K**), 52.89 (**C_A**), 38.34 (**C_I**), 26.42 (**C_J**).

Elemental analysis: L1·H_2O – $C_{26}H_{36}N_6O_7$ (544.89 $gmol^{-1}$) **exp. C** 57.34 **H** 6.66 **N** 15.43 **calc. C** 56.94 **H** 6.63 **N** 15.84.

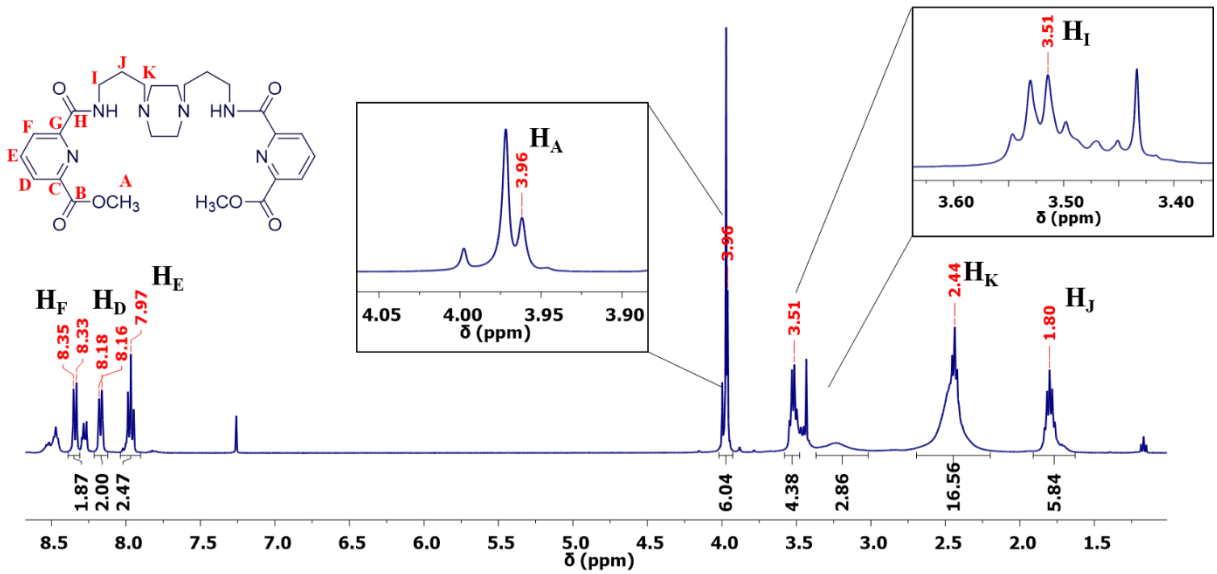

Figure 6.2 – ^{1}H NMR spectrum of **L1**, in $CDCl_3$.

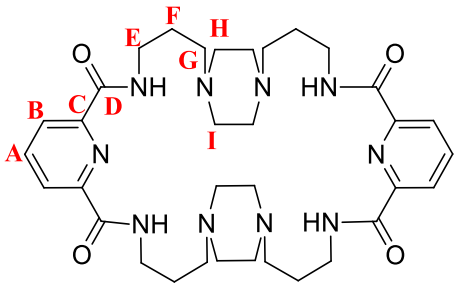

L2

After obtaining the [2+1] product **L1**, the macrocycle [2+2] was synthesised. To 0.909 g (1.73 mmol) of **L1** dissolved in 150 mL of methanol a solution of 1,4-bis(3-aminopropyl)piperazine (355 µL, 1.73 mmol) dissolved in 50 mL of methanol, was added (in one hour and a half) dropwise at room temperature. After the addition, the reaction mixture was refluxed for 24 h. The solvent was evaporated under vacuum and an orange oil was obtained. Petroleum ether was added to the oil and the solvent evaporated multiple time until soft yellow solid was obtained. Mass obtained 0.140 g, yield 45%.

1H NMR (400 MHz, CDCl3, 298 K) δ/ppm: 8.28 (d, J=8.28 Hz 4H, $\mathbf{H_B}$), 7.99 (t, 2H, $\mathbf{H_A}$), 3.41 (s,4H, $\mathbf{H_E}$), 2.74 (t, 4H, $\mathbf{H_{I/H}}$), 1.69 (m, 4H, $\mathbf{H_{H/I}}$), 1.69 (m, 4H, $\mathbf{H_F}$).

13C NMR (100 MHz, CDCl3, 298 K) δ/ppm: 164.26 ($\mathbf{C_D}$), 149.29 ($\mathbf{C_C}$), 139.01 ($\mathbf{C_A}$), 124.93 ($\mathbf{C_B}$), 56.15 ($\mathbf{C_G}$), 40.88 ($\mathbf{C_{I/H}}$), 38.63 ($\mathbf{C_E}$), 29.88 ($\mathbf{C_{H/I}}$), 26.29 ($\mathbf{C_F}$).

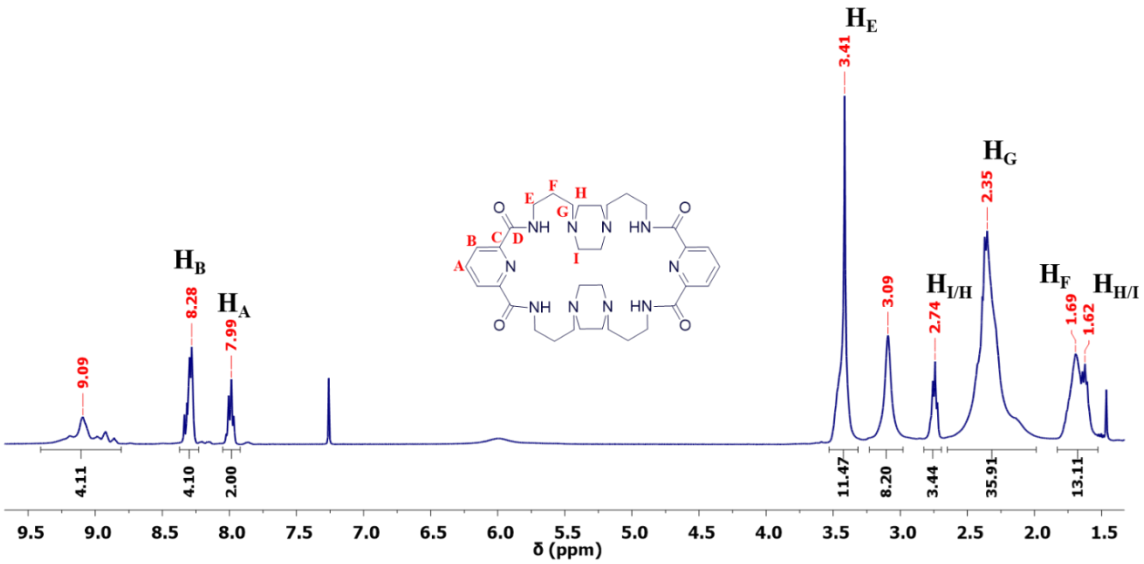

Figure 6.3 – ^{1}H NMR spectrum of **L2**, in $CDCl_3$.

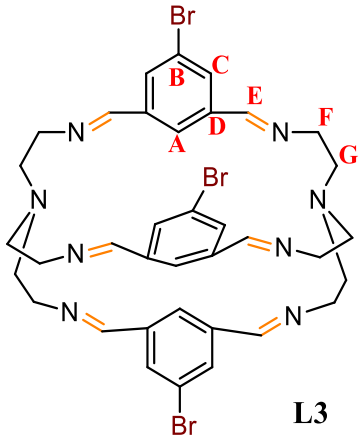

TREN, 0.903 mL (6.04 mmol) was dissolved in 50 mL of methanol and was added dropwise, for 1 h, at room temperature to 1.932 g (9.07 mmol) of bromoisophthalaldehyde dissolved in 1510 mL. The reaction mixture was refluxed for 3 h. Then was concentrated, filtered and washed with methanol and diethyl ether. Mass obtained 1.571 g, yield 63%.

1H NMR (400 MHz, CDCl3, 298 K) δ/ppm: 8.31 (s, 2H, $\mathbf{H_E}$), 7.52 (s, 2H, $\mathbf{H_C}$), 5.38 (s,1H, $\mathbf{H_A}$), 3.78-2.70 (10H, $\mathbf{H_{F/G}}$).

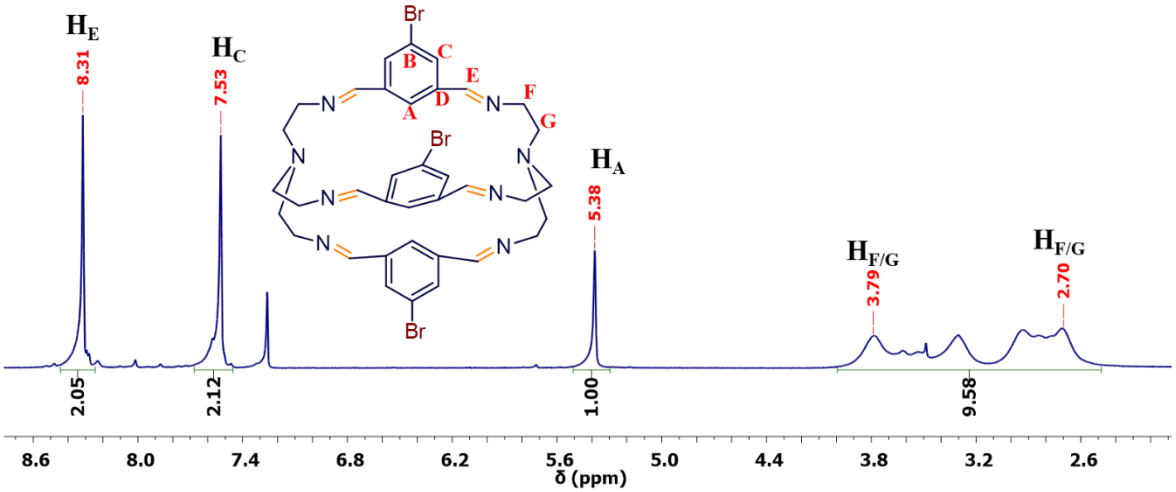

Figure 6.4 – ^{1}H NMR spectrum of **L3**, in $CDCl_3$.

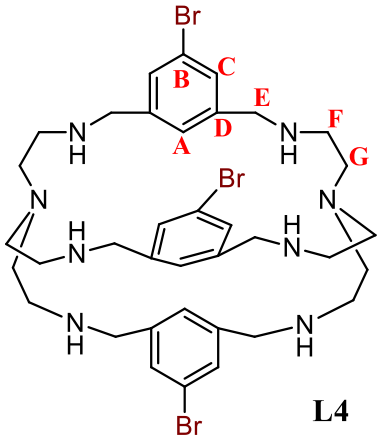

To obtain the **L4** was necessary to reduce the **L3**. 1.405 g (1.70 mmol) of **L3** was dissolved in 18 mL of methanol with acetic acid 10%. The solution was cooled down on an ice bath. Then, 1.072 g (17.06 mmol) of $NaBH_3CN$ was added in small portions and the reaction was stirred overnight, at room temperature. To obtain the product a purification process was needed, a neutral alumina chromatography column of dichloromethane/[methanol/ammonia (9/1)] (0.7:0.04). Mass obtained 0.908 g, yield 64%.

1H NMR (400 MHz, MeOD, 298 K) δ/ppm: 7.51 (s, 2H, $\mathbf{H_C}$), 7.06 (s, 1H, $\mathbf{H_A}$), 3.65 (s,4H, $\mathbf{H_E}$), 2.57 (S,8H, $\mathbf{H_{F/G}}$).

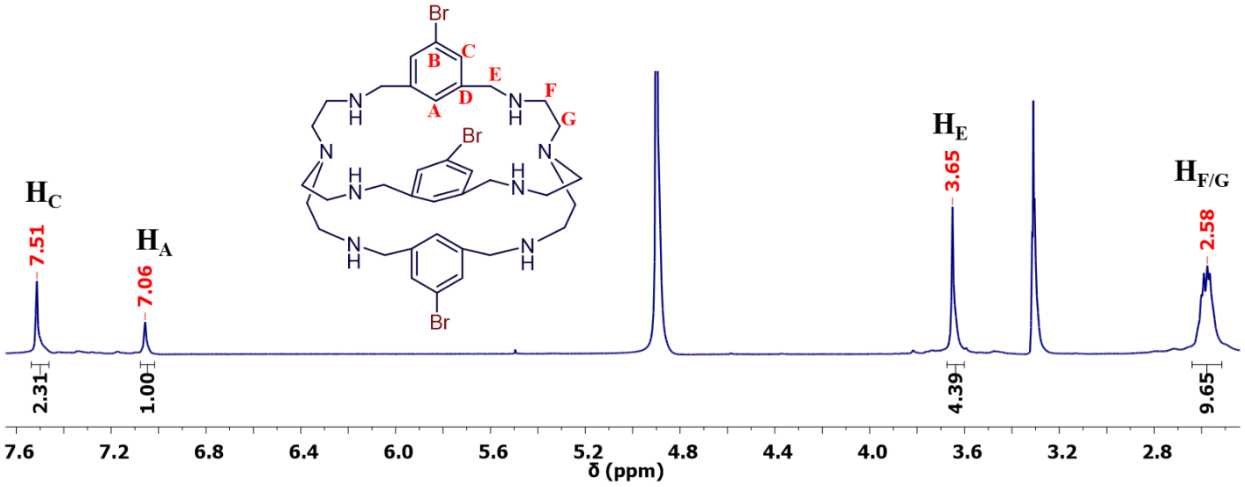

Figure 6.5 – ^{1}H NMR spectrum of **L4**, in MeOD.

6.3.1 Complexes synthesis

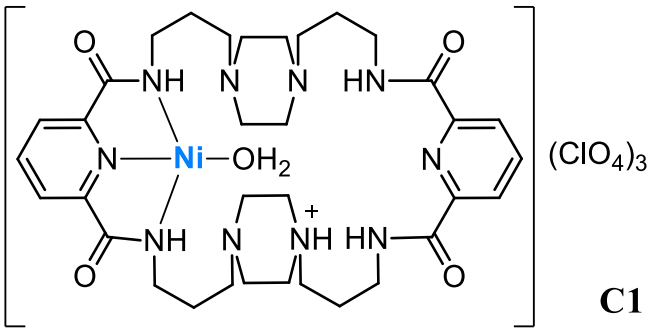

C1

To 0.179 g (0.27 mmol) of **L2** dissolved in 10 mL of methanol $Ni(ClO_4)\cdot 6H_2O$ (0.249 g, 0.680 mmol) dissolved in 10 mL of MeOH was added. The reaction mixture was stirred for 10 min and filtered. The filtrate was left to evaporate in air atmosphere. A yellow paste was obtained, then was washed with diethyl ether and filtered. The result was a yellow powder. Mass obtained 0.140 g, yield 45%.

FTIR (KBr, υ/cm^{-1}): 1631.51 $\upsilon_{(C=O)}$, 1540.87 $\delta_{(N-H)}$, 1087.67 and 624.83 $\upsilon_{(ClO_4^-)}$.

Elemental analysis: C1·7H$_2$O – $C_{34}H_{65}Cl_3N_{10}NiO_{23}$ (1146.99 gmol^{-1}) **exp. C** 35.67 **H** 5.55 **N** 12.23 **calc. C** 35.35 **H** 5.49 **N** 12.46.

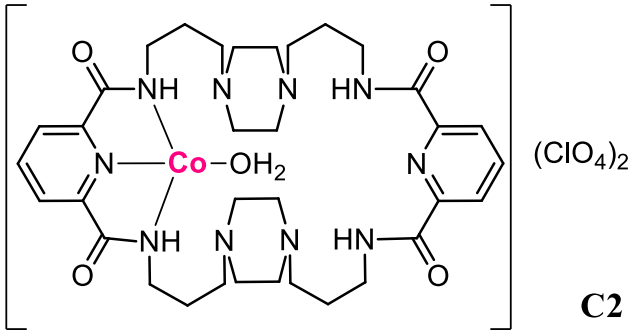

C2

To 0.185 g (0.28 mmol) of **L2** dissolved in 10 mL of methanol $Co(ClO_4)\cdot 6H_2O$ (0.205 g, 0.56 mmol) dissolved in 10 mL of MeOH was added. The reaction mixture was stirred for 10 min and filtered. The filtrate was left to evaporate in air atmosphere. An olive-green paste was obtained, then was washed with diethyl ether and filtered. The result was an olive-green powder. Mass obtained 0.134 g, yield 45%.

FTIR (KBr, υ/cm^{-1}): 1664.29 $\upsilon_{(C=O)}$, 1540.87 $\delta_{(N-H)}$, 1087.67 and 624.83 $\upsilon_{(ClO_4^-)}$.

Elemental analysis: C2·8H$_2$O – $C_{34}H_{66}Cl_2CoN_{10}O_{20}$ (1064.78 gmol^{-1}) **exp. C** 38.35 **H** 6.25 **N** 13.15 **calc. C** 38.38 **H** 5.91 **N** 13.13.

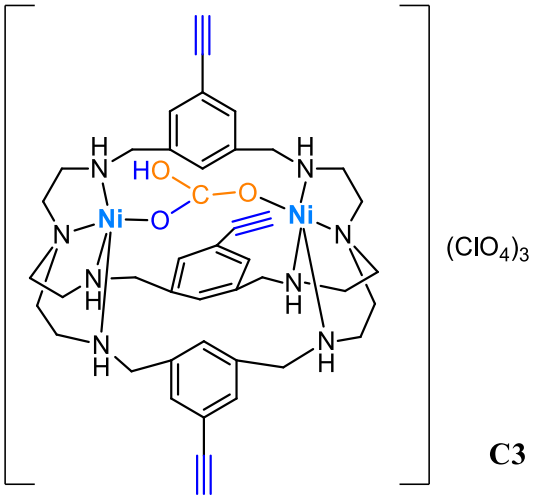

C3

To 0.167 g (0.25 mmol) of **L6** dissolved in 12.5 mL of Ethanol $Ni(ClO_4)\cdot 6H_2O$ (0.167 g, 0.5 mmol) dissolved in a 20 mL mixture (1:1) CH_3CN/EtOH was added. The reaction mixture was stirred for 5 min and then 0.026 g (0.25 mmol) of Na_2CO_3 dissolved in 1-2 mL of water was added. The mixture was stirred for 1 hour. The filtrate was left to evaporate in air atmosphere. Then was washed with ethanol. The result was a blue powder. Mass obtained 0.206 g, yield 70%.

FTIR (KBr, υ/cm^{-1}): 1672 $\upsilon_{(HCO_3^-)}$, 1089.6 and 624.8 cm^{-1} $\upsilon_{(ClO_4^-)}$.

Elemental analysis: C3·CH$_3$CH$_2$OH – $C_{44}H_{60}Cl_3N_8Ni_2O_{16}$ (1180.74 gmol^{-1}) **exp. C** 44.76 **H** 5.12 **N** 9.49 **calc. C** 44.91 **H** 5.08 **N** 9.72.

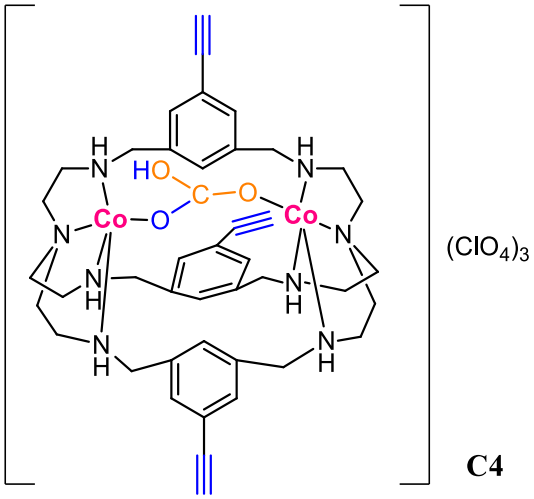

C4

To 0.167 g (0.25 mmol) of **L6** dissolved in 12.5 mL of Ethanol $Co(ClO_4)\cdot 6H_2O$ (0.183 g, 0.5 mmol) dissolved in a 20 mL mixture (1:1) CH_3CN/EtOH was added. The reaction mixture was stirred for 5 min and then 0.026 g (0.25 mmol) of Na_2CO_3 dissolved in 1-2 mL of water was added. The mixture was stirred for 1 hour. The filtrate was left to evaporate in air atmosphere. Then was washed with ethanol a green powder was obtained. Mass obtained 0.154 g, yield 49%.

FTIR (KBr, υ/cm^{-1}): 1635.37 $\upsilon_{(HCO_3^-)}$, 1089.6 and 624.83 cm^{-1} $\upsilon_{(ClO_4^-)}$.

Elemental analysis: C4·2CH$_3$CH$_2$OH·0.75CH$_3$CN – $C_{48.5}H_{66.25}Cl_3Co_2N_{8.75}O_{17}$ (1268.07 gmol^{-1}) **exp. C** 45.79 **H** 4.74 **N** 9.88 **calc. C** 45.94 **H** 5.27 **N** 9.66.

The synthesis of the complexes **C5-C8** were already reported.

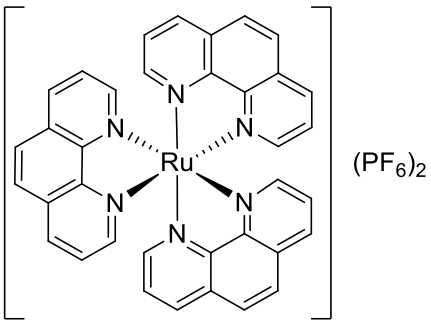

The complex was obtained from a procedure from literature[60] by adding 0.415 g (2 mmol) of $RuCl_3$ and 1.189 g (6 mmol) of 1,10-phenanthroline monohydrated in 30 mL of dry methanol and was refluxed in inert atmosphere 20 hours. The reaction mixture was cooled to room temperature and a solution of NH_4PF_6 in dry methanol. To obtain the product a purification process was needed, a neutral alumina chromatography column of dichloromethane/[methanol/ammonia (9/1)] (0.14:0.04). Mass obtained 0.104 g, Yield 5%.

1H NMR (400 MHz, DMSO, 298 K) δ/ppm: 8.76 (d, J=8.76 Hz, 6H), 8.38 (s, 6H), 8.08 (d, J=8.08 Hz, 7.76 (m, 6H).

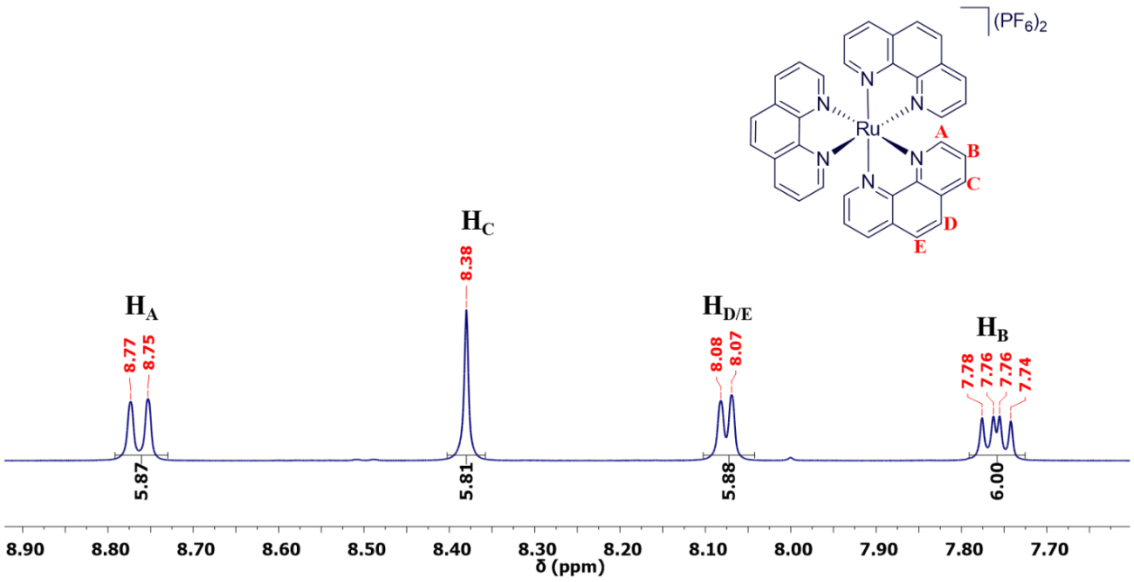

Figure 6.6 – ^1H NMR of $[Ru(phen)_3(PF_6)_2]$, in DMSO.

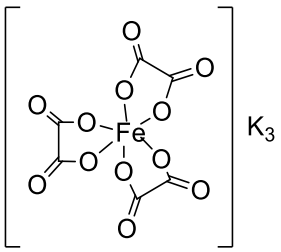

The synthesis was done by a modification in a procedure from literature.[61] The $K_3Fe(C_2O_4)_3$ complex was generated in solution by the addition of 2.007 g (12.33 mmol) of $FeCl_3$ in 8 mL of water in a solution

of 4.543 g (24.66 mmol) of $C_2K_2O_4$ in 16 mL of water, both with a concentration of 1.5 M. The reaction mixture was warmed and stirred 1 h. The reaction stayed on fridge one night then was filtered. Mass obtained 1.125 g, yield 31%.

6.4 MWCNT modification

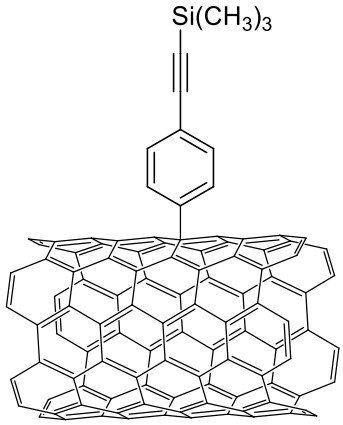

CNT1

MWCNT (200 mg) were suspended in a 20 mM acetonitrile solution of 4-[(Trimethylsilyl)ethynyl]diazonium tetrafluoroborate (40 mL). The suspension was sonicated 20 min and left at 85 ºC overnight. After cooling to room temperature, the modified MWCTN were centrifuged 10 min at 14000 rpm and washed with ethanol and acetone three times each. To dry the MWCNT stayed on an oven at 50 ºC overnight. (194 mg)

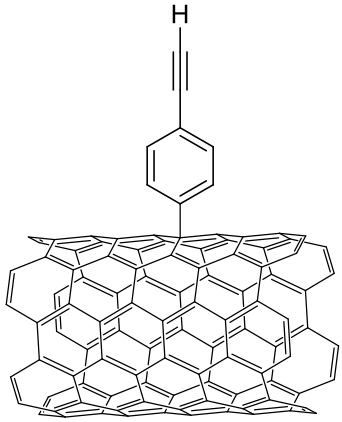

CNT2

CNT1 (194 mg) were suspended in a 0.05 M tetrabutylammonium fluoride in tetrahydrofuran solution (48.5 mL). The mixture was stirred for 3 h and the MWCNT were centrifuged (10 min, 14000 rpm) and washed three times with ethanol and acetone. The MWCNT were dried in the oven at 50 ºC overnight. (143 mg)

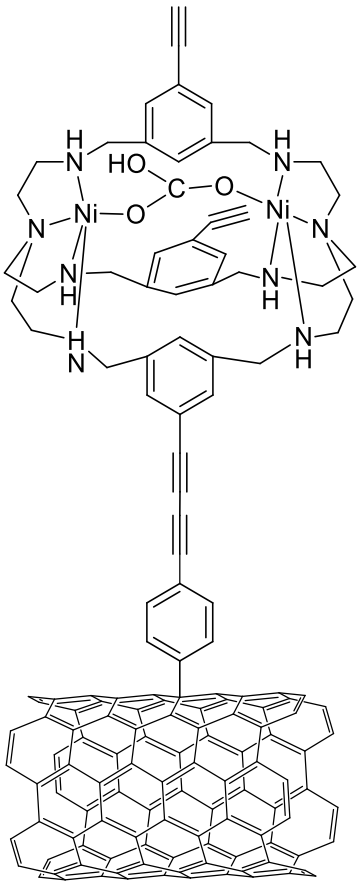

CNT3

CNT2 (30 mg) were suspended in 12 mL of n-methyl pyrrolidone. The suspension was sonicated 20 min and subsequently, 0.113 g (0.096 mmol) of **C3** was added. Next, a newly prepared suspension of 300 µL of TMEDA and 0.074 g (0.75 mmol) of copper(I) chloride in 6 mL of n-methyl pyrrolidone was added. The solution was bubbled for 20 min with compress air, then was stirred, at room temperature, overnight.

The solution was sonicated and washed with NMP, deionized water, a 3% NH_3 solution, deionized water, NMP and deionized water, using a centrifuge at 14.000 for 15 min. The MWCNT were dried in the oven at 50 ºC overnight. (51 mg)

Chapter 7
Bibliography

7. Bibliography

1 W. Macyk, A. Franke and G. Stochel, *Coord. Chem. Rev.*, 2005, **249**, 2437–2457.

2 F. Möller, S. Piontek, R. G. Miller and U. P. Apfel, *Chem. Eur. J.*, 2018, **24**, 1471–1493.

3 G. A. Melson, *Coordination Chemistry of Macrocyclic Compounds*, Plenum Press, New York, 1979.

4 T. J. Hubin, *Coord. Chem. Rev.*, 2003, **241**, 27–46.

5 C. J. Pedersen, *J. Am. Chem. Soc.*, 1967, **89**, 7017–7036.

6 G. Ferraudi, J. C. Canales, B. Kharisov, J. Costamagna, J. G. Zagal, G. Cardenas-Jirón and M. Paez, *J. Coord. Chem.*, 2005, **58**, 89–109.

7 M. Schroder, *Pure Appl. Chem.*, 1988, **60**, 517–524.

8 E. L. Gavey and M. Pilkington, *Coord. Chem. Rev.*, 2015, **296**, 125–152.

9 H. Bhakhoa, L. Rhyman, E. P. Lee, D. K. W. Mok, P. Ramasami and J. M. Dyke, *Dalton Trans.*, 2017, **46**, 15301–15310.

10 J. W. Steed and J. L. Atwood, *Supramolecular Chemistry*, Wiley, 1st Ed., 2000.

11 J. S. Bradshaw, *Aza-Crown Macrocycles*, 1993.

12 X. Zhang, D. Huang, Y. S. Chen and R. H. Holm, *Inorg. Chem.*, 2012, **51**, 11017–11029.

13 Y. Matano, *Chem. Rev.*, 2017, **117**, 3138–3191.

14 B. Dietrich, J. M. Lehn and J. P. Sauvage, *Tetrahedron Lett.*, 1969, **10**, 2889–2892.

15 G. M. Mamardashvili, O. V. Maltceva, N. Z. Mamardashvili, N. T. Nguyen and W. Dehaen, *RSC Adv.*, 2015, **5**, 44557–44562.

16 C. J. Harding, Q. Lu, J. F. Malone, D. J. Marrs, N. Martin, V. Mckee and J. Nelson, *J. Am. Chem. Soc.*, 1995, 1739–1747.

17 B. C. J. Moulton and B. L. Shaw, *Dalton Trans.*, 1976, **0**, 1020–1024.

18 D. Morales-Morales, *Rev. Soc. Quim. Mex.*, 2004, **48**, 338–346.

19 K. M. Schultz, K. I. Goldberg, D. G. Gusev and D. M. Heinekey, *Organometallics*, 2011, **30**, 1429–1437.

20 R. J. Rubio, G. T. S. Andavan, E. B. Bauer, T. K. Hollis, J. Cho, F. S. Tham and B. Donnadieu, *J. Organomet. Chem.*, 2005, **690**, 5353–5364.

21 H. P. Dijkstra, M. D. Meijer, J. Patel, R. Kreiter, G. P. M. Van Klink, M. Lutz, A. L. Spek, A. J. Canty and G. Van Koten, *Organometallics*, 2001, **20**, 3159–3168.

22 C. M. Hartshorn and P. J. Steel, *Organometallics*, 1998, **17**, 3487–3496.

23 D. M. Spasyuk, S. I. Gorelsky, A. Van Der Est and D. Zargarian, *Inorg. Chem.*, 2011, **50**, 2661–2674.

24 E. Poverenov, M. Gandelman, L. J. W. Shimon, H. Rozenberg, Y. Ben-David and D. Milstein, *Organometallics*, 2005, **24**, 1082–1090.

25 M. Mehring, M. Schürmann and K. Jurkschat, *Organometallics*, 1998, **17**, 1227–1236.

26 M. Doux, C. Bouet, N. Mezailles, L. Ricard and P. Le Floch, *Organometallics*, 2002, **21**, 2785–

2788.

27 D. Huang and R. H. Holm, Chem. Eur. J., 2010, 6242–6250.

28 D. Huang, O. V Makhlynets, L. L. Tan, S. C. Lee, E. V Rybak-akimova and R. H. Holm, Inorg. Chem., 2011, **50**, 10070–10081.

29 D. Huang, O. V Makhlynets, L. Ling, S. C. Lee, E. V Rybak-akimova and R. H. Holm, Proc. Acad. Sci. U.S.A , 2011, **108**, 1222–1227.

30 O. Troeppner, D. Huang, R. H. Holm and I. Ivanovic-Burmazovic, *Dalton Trans.*, 2014, **43**, 5274–5279.

31 Q. Q. Wang, V. W. Day and K. Bowman-James, *Org. Lett.*, 2014, **16**, 3982–3985.

32 G. L. Guillet, J. B. Gordon, G. N. Di Francesco, M. W. Calkins, E. Čižmár, K. A. Abboud, M. W. Meisel, R. García-Serres and L. J. Murray, *Inorg. Chem.*, 2015, **54**, 2691–2704.

33 Y. Dussart, C. Harding, P. Dalgaard, C. McKenzie, R. Kadirvelraj, V. McKee and J. Nelson, *J. Chem. Soc. Dalton Trans.*, 2002, 1704–1713.

34 N. J. English, M. M. El-Hendawy, D. A. Mooney and J. M. D. MacElroy, *Coord. Chem. Rev.*, 2014, **269**, 85–95.

35 J.-M. Chen, W. Wei, X.-L. Feng and T.-B. Lu, *Chem. Asian J.*, 2007, **2**, 710–719.

36 H. Rao, J. Bonin and M. Robert, *Chem. Commun.*, 2017, **53**, 2830–2833.

37 Z. Guo, S. Cheng, C. Cometto, E. Anxolabéhère-Mallart, S.-M. Ng, C.-C. Ko, G. Liu, L. Chen, M. Robert and T.-C. Lau, *J. Am. Chem. Soc.*, 2016, **138**, 9413–9416.

38 T. Ouyang, H. H. Huang, J. W. Wang, D. C. Zhong and T. B. Lu, *Angew. Chem. Int. Ed.*, 2017, **56**, 738–743.

39 A. J. Morris, G. J. Meyer and E. Fujita, *Acc. Chem. Res.*, 2009, **42**, 1983–1994.

40 H. Takeda, C. Cometto, O. Ishitani and M. Robert, *ACS Catal.*, 2017, **7**, 70–88.

41 A. Maurin and M. Robert, *Chem. Commun.*, 2016, **52**, 12084–12087.

42 S. Realista, PhD thesis, Universidade de Lisboa, 2018.

43 W. Q. Ong, H. Zhao, Z. Du, J. Z. Y. Yeh, C. Ren, L. Z. W. Tan, K. Zhang and H. Zeng, *Chem. Commun.*, 2011, **47**, 6416–6418.

44 I. V Korendovych, M. Cho, P. L. Butler, R. J. Staples and E. V Rybak-akimova, *Org. Lett.*, 2006, **8**, 3171–3174.

45 P. Vollhardt and N. Schore, *Organic Chemistry Structure and Function*, New York, NY: Freeman and Company, 7th Ed., 2014.

46 R. M. Silverstein and F. X. Webster, *Spectrometric Identification of Organic Compounds*, John Wiley & Sons, Inc., 6th Ed., 1998.

47 P. Larkin, *Infrared Raman Spectrosc.*, 2011, 117–133.

48 Y. R. Leroux, H. Fei, J. M. Noël, C. Roux and P. Hapiot, *J. Am. Chem. Soc.*, 2010, **132**, 14039–14041.

49 S. Anderson, *Chem. Eur. J.*, 2001, **7**, 4706–4714.

50 I. Hijazi, T. Bourgeteau, R. Cornut, A. Morozan, A. Filoramo, J. Leroy, V. Derycke, B. Jousselme and S. Campidelli, *J. Am. Chem. Soc.*, 2014, **136**, 6348–6354.

51 F. Strauß, H. Erwin, P. Heitjans, V. Trouillet and M. Bruns, *RSC Adv. Open*, 2015, **5**, 7192–7195.

52 K.-I. Aika and K. Aono, *J. Chem. Soc. Faraday Trans.*, 1991, **87**, 1273–1277.

53 J. Russat, *Surf. Interface Anal.*, 1988, **11**, 414–420.

54 C. Ji, S. Yin, S. Sun and S. Yang, *Appl. Surf. Sci.*, 2018, **434**, 1224–1231.

55 T. Yoshida, K. Yamasaki and S. Sawada, *Bull. Chem. Soc. Jpn*, 1978, **51**, 1561–1562.

56 A. P. S. Roseiro, P. Adão, A. M. Galvão, J. Costa Pessoa, A. M. Botelho Do Rego and M. F. N. N. Carvalho, *Inorg. Chem. Front.*, 2015, **2**, 1019–1028.

57 C. W. Machan, M. D. Sampson and C. P. Kubiak, *J. Am. Chem. Soc.*, 2015, **137**, 8564–8571.

58 S. Aoi, K. Mase, K. Ohkubo and S. Fukuzumi, *Catal. Sci. Technol.*, 2016, **6**, 4077–4080.

59 P. G. Alsabeh, A. Rosas-Hernández, E. Barsch, H. Junge, R. Ludwig and M. Beller, *Catal. Sci. Technol.*, 2016, **6**, 3623–3630.

60 W. Wang, J. Zhang, H. Wang, L. Chen and Z. Bian, *Appl. Catal. A Gen.*, 2016, **520**, 1–6.

61 D. Collison and A. K. Powell, *Inorg. Chem.*, 1990, **29**, 4735–4746.

Chapter 8
Annexes

8. Annexes

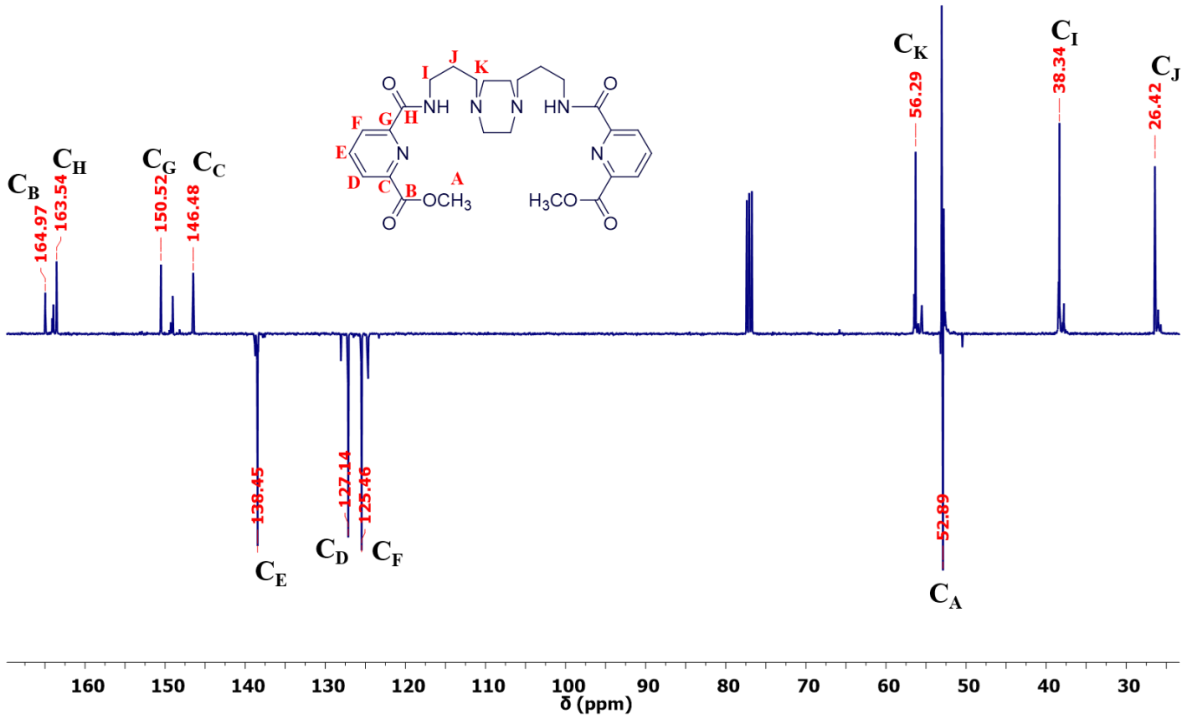

Figure 8.1 – ^{13}C-APT NMR spectrum of **L1**, in $CDCl_3$.

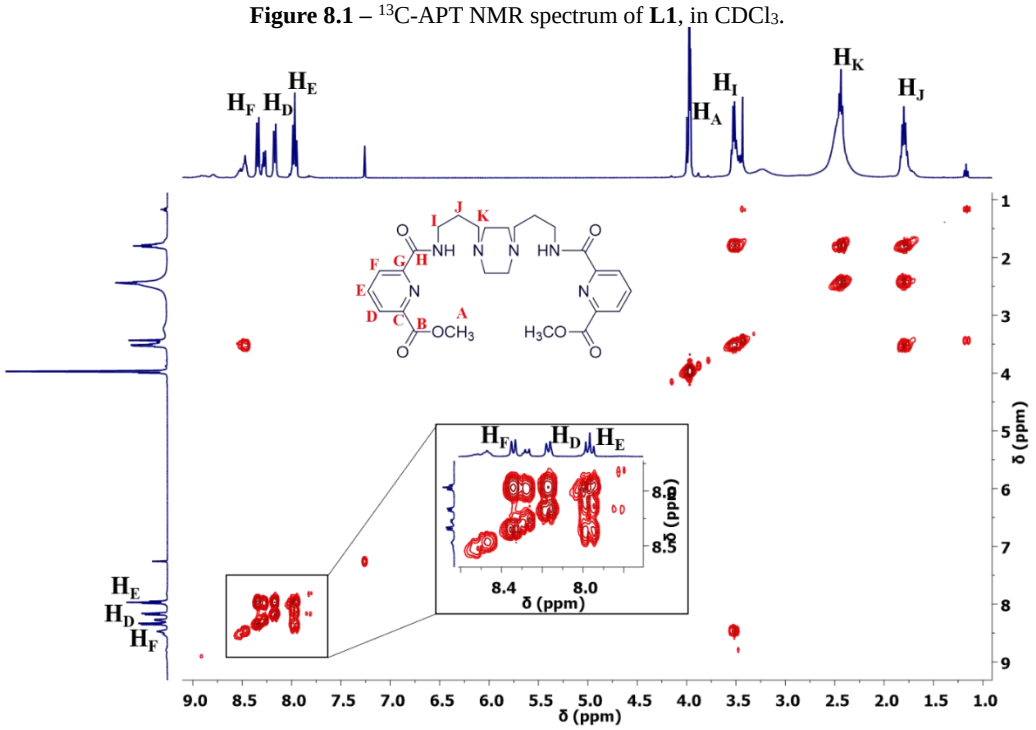

Figure 8.2 – COSY NMR spectrum of **L1**, in $CDCl_3$.

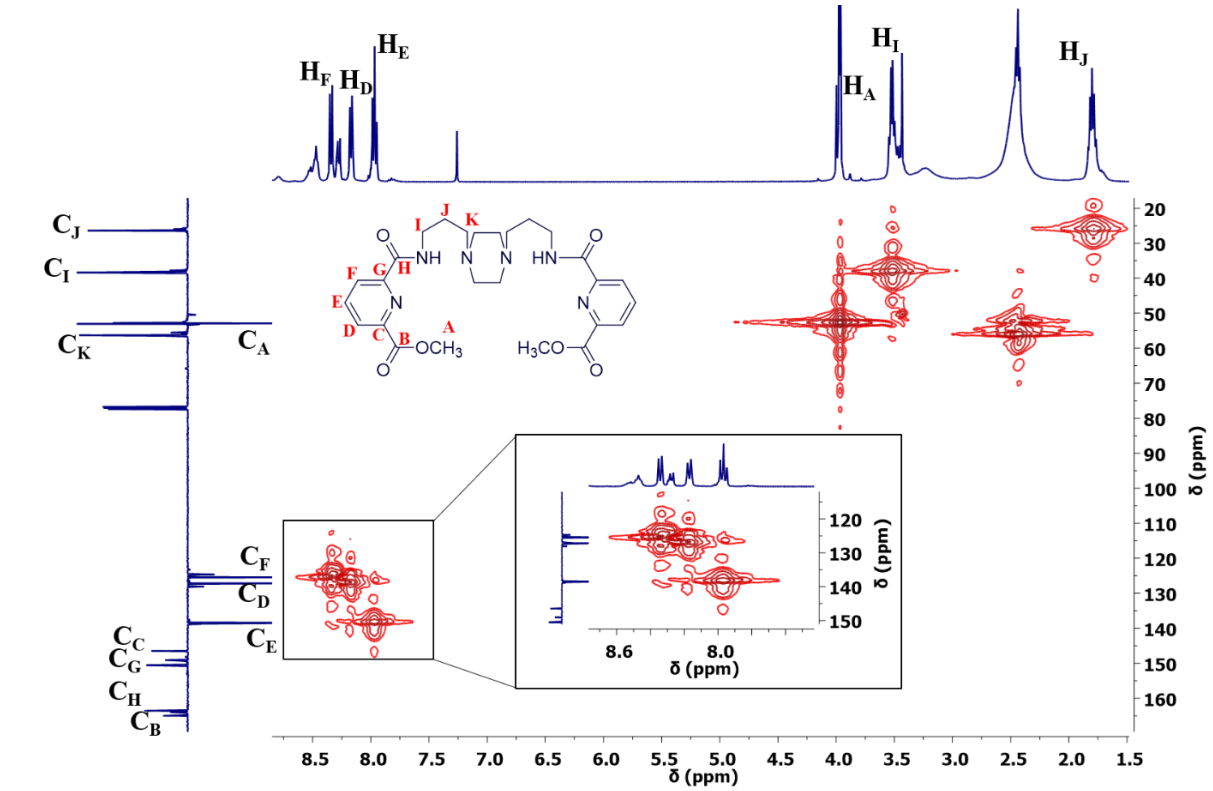

Figure 8.3 – HMQC NMR spectrum of **L1** in $CDCl_3$.

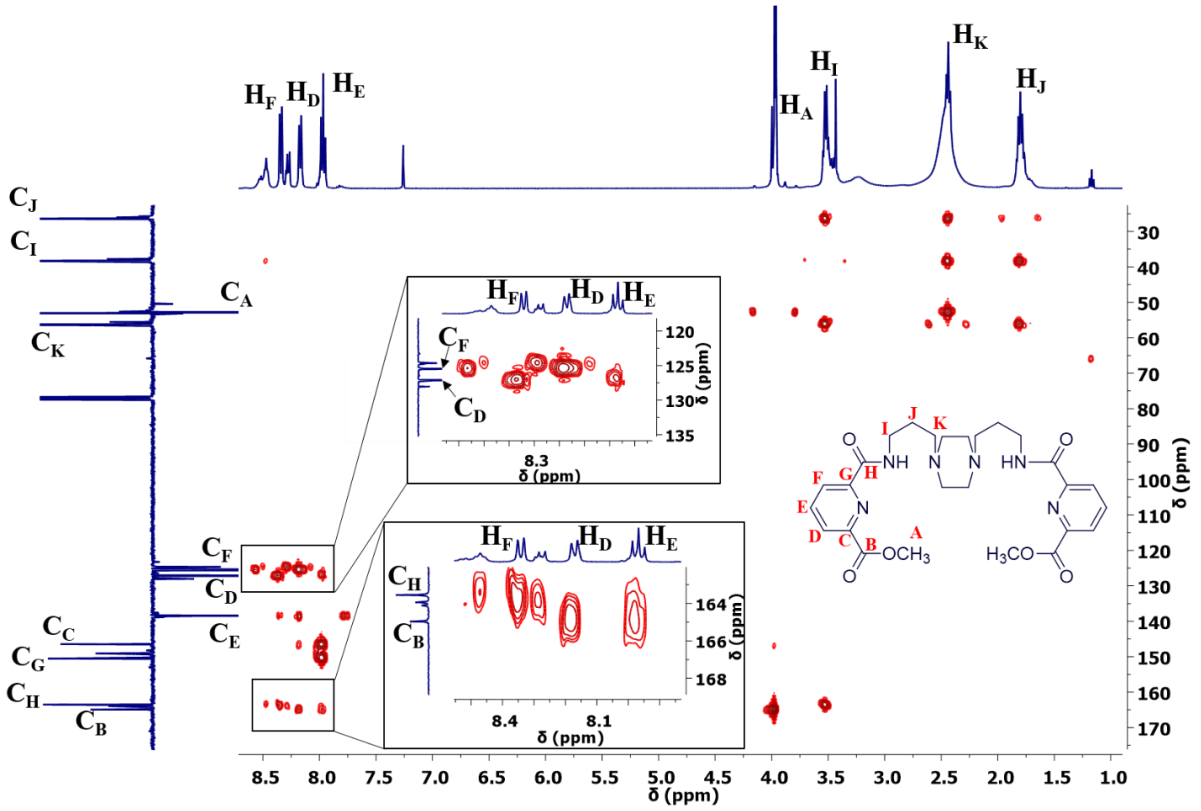

Figure 8.4 – HMBC NMR spectrum of **L1** in $CDCl_3$.

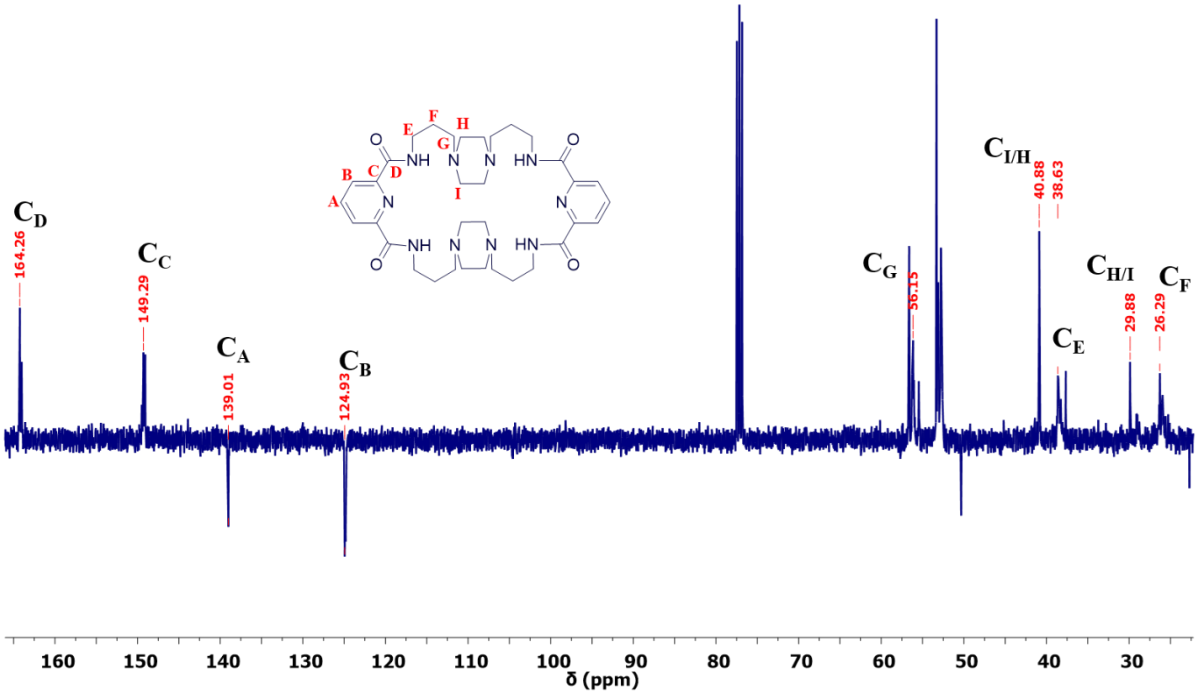

Figure 8.5 – ^{13}C-APT NMR spectrum of **L2**, in $CDCl_3$.

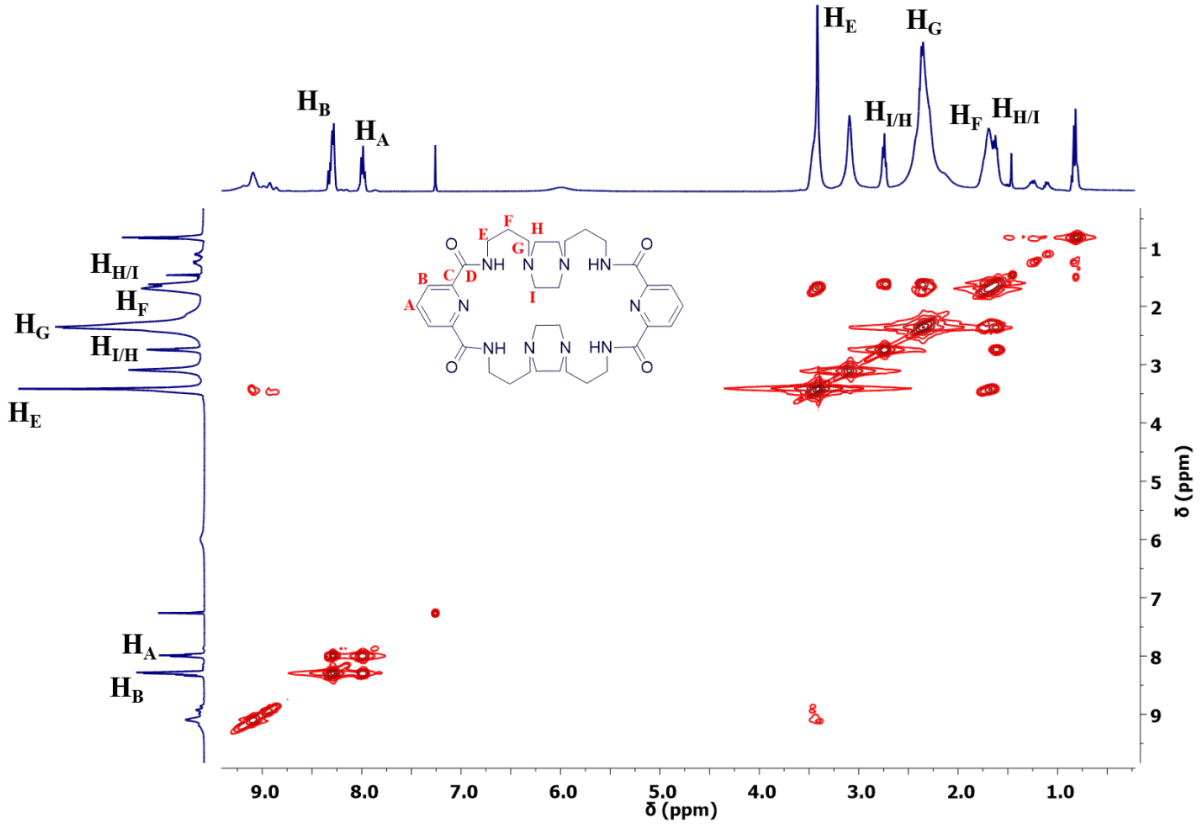

Figure 8.6 – COSY NMR spectrum of **L2**, in $CDCl_3$.

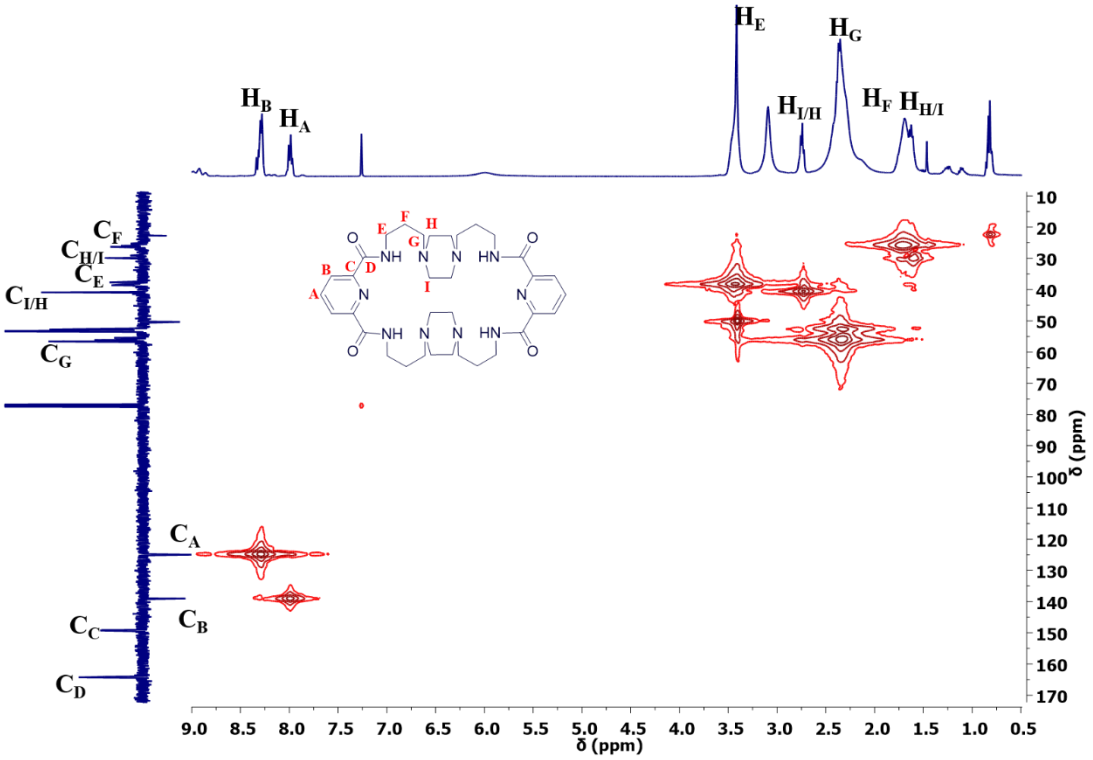

Figure 8.7 – HMQC NMR spectrum of **L2**, in $CDCl_3$.

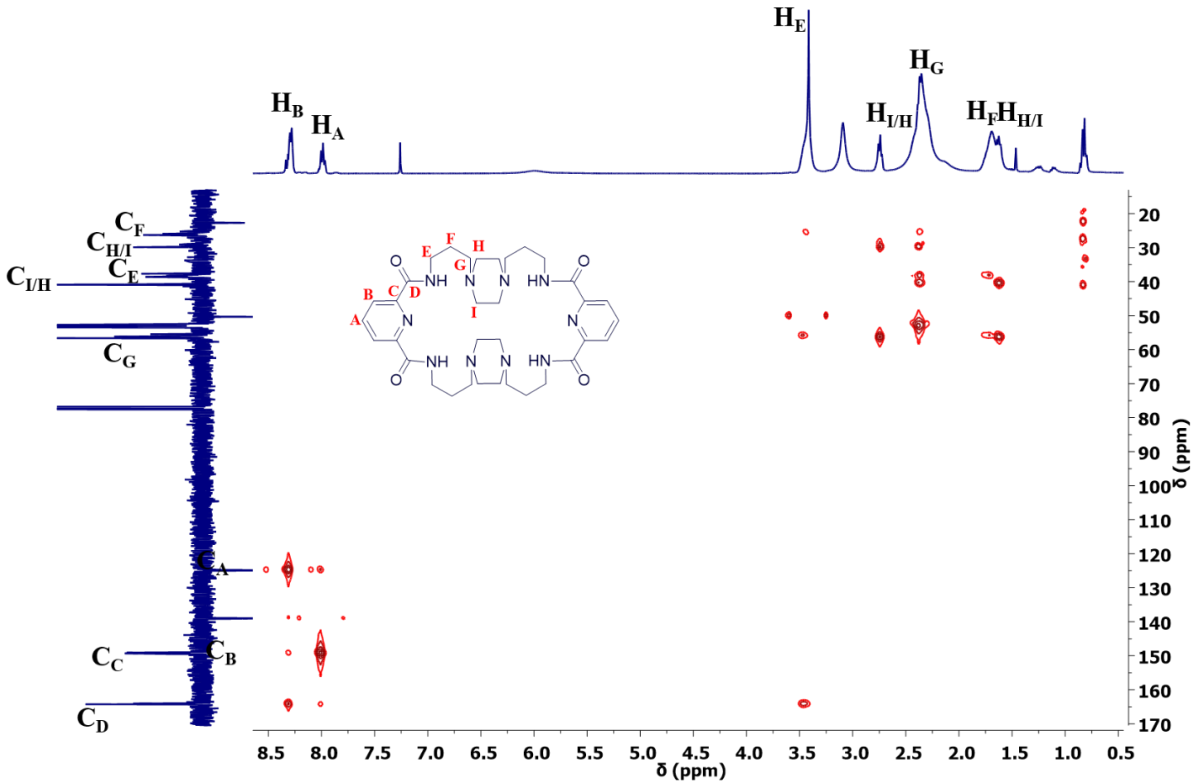

Figure 8.8 – HMBC NMR spectrum of **L2**, in $CDCl_3$.

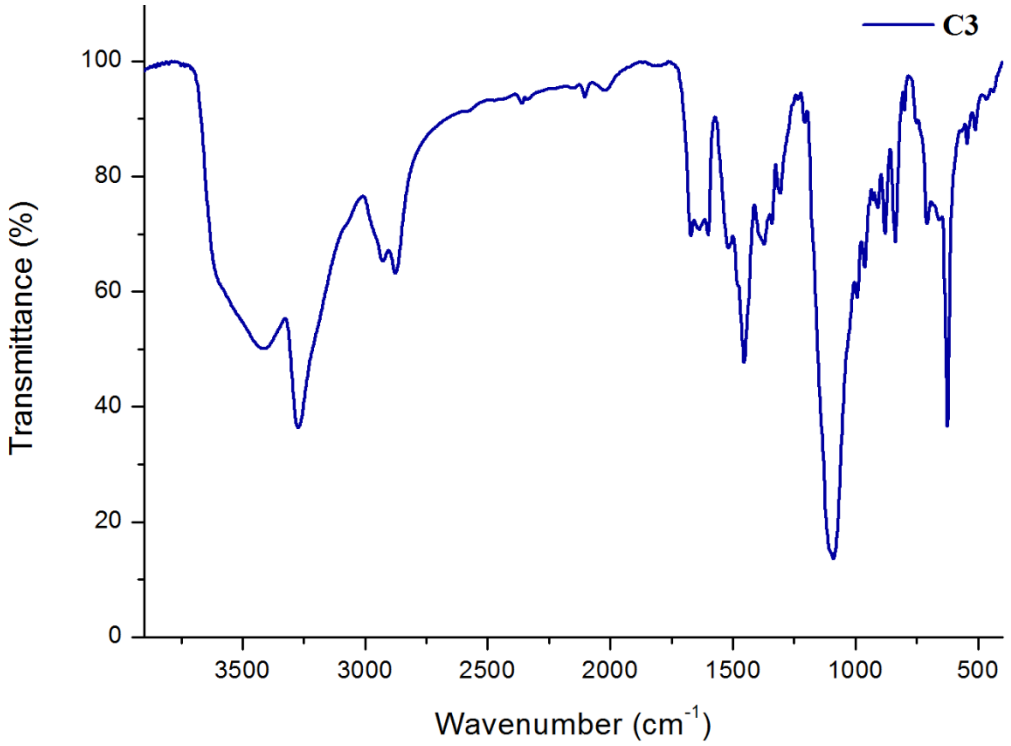

Figure 8.9 – FTIR spectrum of the complexes **C3**.

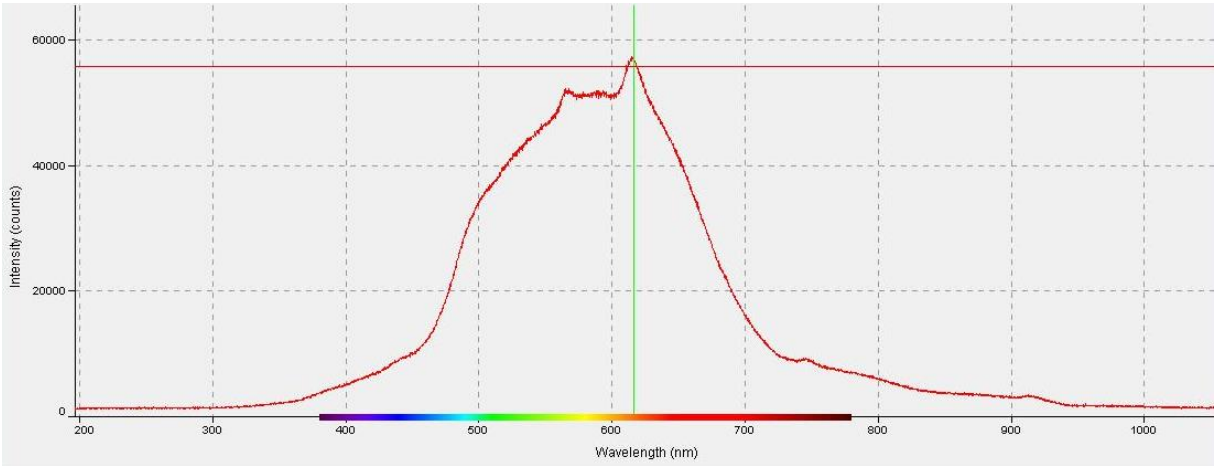

Figure 8.10 – Solar light simulator spectrum.